RESULTS

HIV-1 Genotype Distribution in Malaysia

HIV-1 genotypes circulating among various risk populations (n = 184) were determined by phylogenetic and recombination breakpoint analyses based on the nucleotide sequences of the Pro and RT regions. Distribution of HIV-1 genotypes in Malaysia is currently as follows: CRF01_AE (105/184, 57.1%), subtype B′ (37/184, 20.1%), and subtype C (1/184, 0.5%) (Fig. 2). A substantial proportion (41/184, 22.3%) of specimens showed unique subtype structure composed of CRF01_AE and subtype B.[23,24] The majority of them (35/184, 19.0%) harbored the identical subtype structure, and a small proportion of specimens (6/184, 3.3%) displayed different profiles of recombinant structure. We designate these two groups of Malaysian HIV-1 recombinant strains as the major recombinant form (major RF) and the minor RF, respectively. The prevalence of the major RF was highest among IDUs (42.0%, 21/50), but it was also found among other risk populations: male homo-/bisexuals (18.8%, 3/16) and heterosexuals (9.8%, 9/92; Fig. 2).

Near-Full-Length Nucleotide Sequence Analysis Detects New CRF in Malaysia

To characterize the detailed subtype structure of new HIV-1 recombinant strains in Malaysia, we determined near-full-length nucleotide sequences of HIV-1 strains from eight epidemiologically unlinked individuals who are infected with

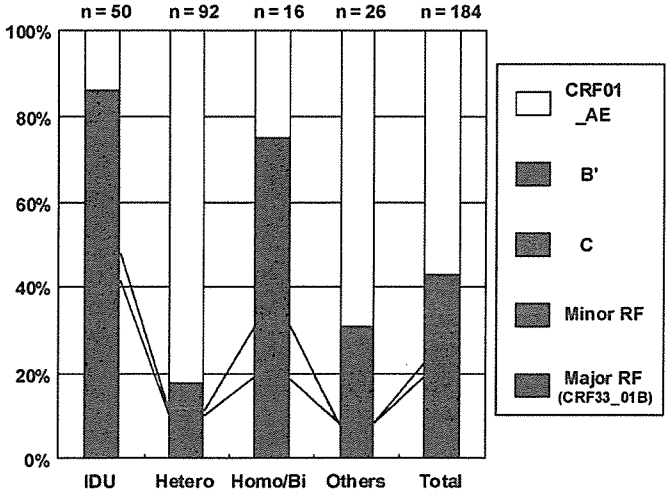

FIGURE 2. Distribution of HIV-1 genotypes in different risk groups in Malaysia. Genotypes were determined by phylogenetic and recombination breakpoint analyses of the nucleotide sequences in protease and reverse transcriptase regions (see text). Bars indicate the relative frequency (%) of HIV-1 genotypes in each risk group shown at the bottom. "n" indicates the number of specimens analyzed in each risk group. "Others" include 22 cases with unknown risk factors and 4 cases of MCT. Abbreviations: B′, HIV-1 subtype B′ (Thai variant of subtype B); C, subtype C; major RF, major recombinant forms (CRF33_01B); minor RF, minor recombinant forms (unique recombinant forms composed of CRF01_AE and subtype B).

either major RFs (n = 4) (05MYKL007.1, 05MYKL015.2, 05MYKL031.1, and 05MYKL045.1) or minor RFs (n = 4) (04MYKL016.1, 03MYKL018.1, 04MYKL019.1, and 05MYKL043.1) (Table 1). The bootscanning plot of near-full-length nucleotide sequences revealed that four major RFs indeed displayed the identical recombinant structure composed of CRF01_AE and subtype B (Fig. 3A). In this chimera, two short subtype B segments are inserted into a backbone of CRF01_AE. The profile of the subtype structure of Malaysian major RFs is distinct from that of CRF15_01B previously reported in Thailand,[19] where most of the *env* region belongs to subtype B in a backbone of CRF01_AE (Figs. 3B, C). In major RFs, a total of four recombination breakpoints (sites I–IV in Fig. 3C) are found to be clustered in a 0.9-kb region in *gag*-RT gene. The subregion tree analysis demonstrated that CRF01_AE segments (regions 1 and 5 in Fig. 3B) in major RFs belonged to the cluster of Thailand CRF01_AE, indicating that these segments indeed originated from CRF01_AE of Thai origin. However, region 3 (121 bp) was too short to discern its origin from either African or Thailand CRF01_AEs. Similarly, we were not able to discern whether subtype B segments (regions 2 and 4) originated from subtype B′ because subtypes B and B′ are phylogenetically indistinguishable in the Pro-RT region (Fig. 3B).

On the other hand, minor RFs (n = 4) showed a different degree of structural relatedness with major RFs. In particular, site II in Pro region is shared between major RFs and three minor RFs (1.6%, 3/184) (04MYKL016.1, 04MYKL019.1, and 05MYKL043.1; Fig. 3C). Similarly, the recombination breakpoints in *gag* p7 (site I) and RT (site IV) regions in major RF are shared with 04MYKL016.1 and 05MYKL043.1, respectively. 03MYKL018.1 is the most distantly related recombinant that shows no obvious structural relatedness with other RFs, while 05MYKL043.1 is most closely related with major RFs, sharing two recombination breakpoints (sites II and IV) but harboring slightly longer subtype B segments in *gag*-Pro and Pro-RT regions than major RFs (Fig. 3C).

Consistent with the results of recombination breakpoint analyses, the phylogenetic tree analysis of near-full-length nucleotide sequences showed that four major RFs (05MYKL007.1, 05MYKL015.2, 05MYKL031.1, and 05MYKL045.1) and the most closely related minor RF (05MYKL043.1) formed a monophyletic cluster with high bootstrap values (93%) (Fig. 3D). In contrast, three other minor RFs (04MYKL016.1, 03MYKL018.1, and 04MYKL019.1) are located outside any of the CRF01_AE-related sequences, including CRF15_01B (Fig. 3D).

Characterization of the Recombination Breakpoints in Malaysian RFs

To search for the possible sequence signatures near the subtype boundaries in Malaysian RFs, we mapped out all four recombination breakpoints (sites I–IV in Fig. 3C) estimated by informative site analysis (Fig. 4). It is noted that the homopolymeric nucleotide tracts (polyadenine ($A_{\geq 4}$), polyguanine ($G_{\geq 3}$), polycytosine ($C_{\geq 4}$), or polythymine ($T_{\geq 4}$)), known to pause in vitro reverse transcription and promote template switch,[32,33] are observed within or adjacent to all four recombination breakpoints. In particular, a characteristic

TABLE 1. Epidemiological and Clinical Background of Study Subjects Harboring Novel CRF01_AE/B Recombinants Emerging in Malaysia

Sample ID	Sex	Age (y)	Ethnicity	Risk Factor*	Date of First Positive HIV-1 Test (mo/yr)	Date of Collection (mo/yr)	Treatment Status†
05MYKL007.1	Male	32	Chinese	Homo	11/04	6/05	ARV-naive
05MYKL015.2	Male	33	Malay	Homo	4/04	8/05	ARV-naive
05MYKL031.1	Male	44	Indian	Hetero	1/05	8/05	3TC d4T NVP
05MYKL045.1	Male	43	Malay	Hetero	7/05	8/05	AZT 3TC EFV
04MYKL016.1	Female	30	Malay	Hetero	9/02	4/04	ARV-naive
03MYKL018.1	Male	32	Chinese	Bisexual	1/97	12/03	ARV-naive
04MYKL019.1	Male	49	Chinese	Hetero + IDU	2/04	6/04	ARV-naive
05MYKL043.1	Male	32	Malay	Hetero + IDU	8/03	8/05	AZT 3TC EFV

Sample ID	CD4 Count (cells/mm^3)	Viral Load (copies/mL)	Specimen Type	HIV-1 Genotype‡	Accession No.
05MYKL007.1	389	14,300	Isolate	CRF33_01B	DQ366659
05MYKL015.2	310	9,900,000	Isolate	CRF33_01B	DQ366660
05MYKL031.1	3	188,000	Isolate	CRF33_01B	DQ366661
05MYKL045.1	121	4300	Isolate	CRF33_01B	DQ366662
04MYKL016.1	401	3290	Plasma	Minor RF	DQ366663
03MYKL018.1	74	328,000	Plasma	Minor RF	DQ366664
04MYKL019.1	78	67,100	Plasma	Minor RF	DQ366665
05MYKL043.1	375	<50	Isolate	Minor RF	DQ366666

*Homo indicates male homosexual; Hetero, heterosexual; IDU, injecting drug user.
†ARV indicates antiretroviral; 3TC, lamivudine; d4T, didanosine; NVP, nevirapine; AZT, zidovudine; EFV, efavirenz.
‡Minor RF refers to the unique recombinant form composed of CRF01_AE and subtype B that showed a different degree of structural relatedness with CRF33_01B (Fig. 3).

homopolymeric nucleotide tract, the A_6GA_6 sequence, was found within site IV (in the RT gene). Similarly, noncontiguous sets of homopolymeric tracts, $A_5/G_5/T_4$ sequence, were observed within site II (in Pro gene). It is also noted that sites I and III are located adjacent to the boundaries between *gag* p7 and p1 and between Pro and RT, respectively (Fig. 4).

DISCUSSIONS

In the present study, we identified a novel CRF (CRF33_01B) composed of CRF01_AE and subtype B in Malaysia. Four sets of near-full-length nucleotide sequences with identical recombinant structure were determined from epidemiologically unlinked individuals with different risk factors and ethnicities in Malaysia (Table 1). This new chimera displays the recombinant structure distinct from any other CRFs reported to date, including CRF15_01B identified in Thailand.[19] The prevalence of CRF33_01B was particularly high among IDUs (42.0%, 21/50), compared with other risk populations (18.8% (3/16) in male homo-/bisexuals; 9.8% (9/92) in heterosexuals; Fig. 2). This may suggest that CRF33_01B first emerged among IDUs and subsequently spread to other risk populations.[23,24]

In addition to this new CRF33_01B, we detected six minor RFs consisting of CRF01_AE and subtype B. Among them, we determined the near-full-length nucleotide sequences of four minor RFs (Table 1). Most of them (except 03MYKL018.1) seem to share the recombination breakpoints with those of CRF33_01B (Fig. 3C). This suggests that they are closely related relatives and are most likely to be secondary recombinants derived from CRF33_01B that were generated by subsequent crossover(s) with either CRF01_AE or subtype B strain circulating in Malaysia.

The sequence characteristics found in or near the recombination breakpoints in CRF33_01B are suggestive of the following traits: (i) The homopolymeric tracts, known to pause in vitro reverse transcription and promote template switch (retroviral recombination),[32,33] are detected within or adjacent to all four recombination breakpoints in CRF33_01B (sites I–IV in Fig. 3C). Particularly, site II recombination breakpoint in Pro gene that contains a characteristic set of noncontiguous homopolymeric tracts, $A_5/G_5/T_4$ sequence (Fig. 4), was shared with three out of four minor RFs (05MYKL043.1, 04MYKL016.1, and 04MYKL019.1; Fig. 3C). Interestingly, this recombination breakpoint (site II) is shared with some of CRF01_AE/B recombinants reported in Thailand (unpublished data). It is thus tempting to speculate that site II may be one of the preferred sites for in vivo recombination. (ii) Some recombination breakpoints are found near the boundaries of functional domains of HIV-1 proteins: sites I and III are located adjacent to the boundaries between *gag* p7 and p1 and between Pro and RT, respectively (Fig. 4). This may reflect the selection pressure to maintain the functional integrity of HIV-1 proteins in recombination processes. Extensive dissemination of this new CRF over CRF01_AE and subtype B particularly among IDUs in Malaysia may suggest the presence of yet undefined selective advantages over parental strains.

Finally, we observed a unique parallelism of the transition in molecular epidemiological features of HIV-1

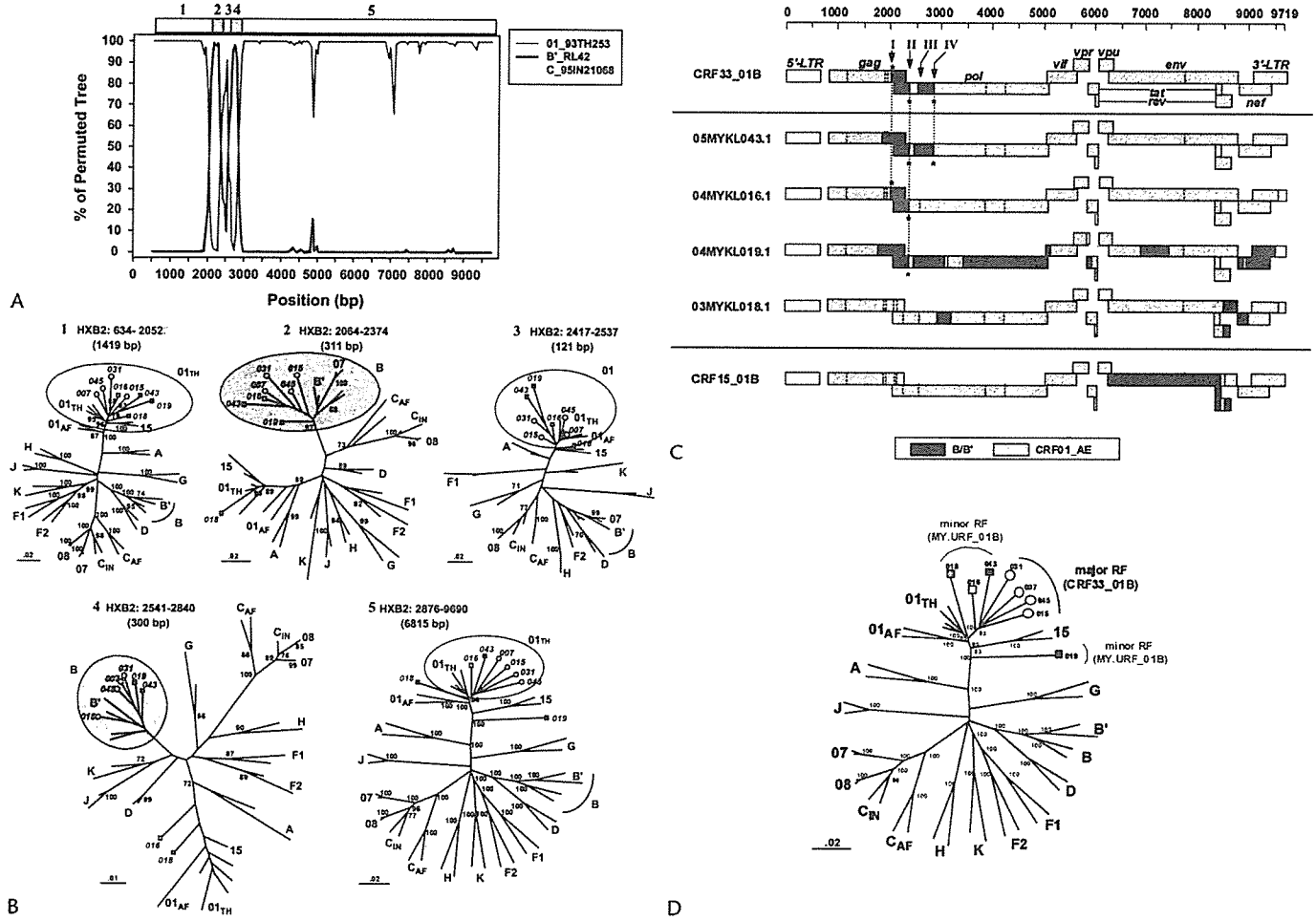

FIGURE 3. Characterization of newly emerging HIV-1 recombinant forms (RFs) in Malaysia. A, Bootscanning analysis of major RF (CRF33_01B). CRF01.93TH253 and B′. RL42 are used as the putative parental subtypes. Bootstrap values of 100 replicates were plotted for a window of 250 bp moving in increments of 50 bp along near-full-length sequences. B, Subregion trees in the segments (1–5) defined by informative site analysis of CRF33_01B are illustrated. Nucleotide positions of each segment relative to HXB2 and the size of segments (in parentheses) are indicated. Bootstrap values (≥70%) are shown. Major RFs (CRF33_01B) (n = 4: 05MYKL007.1, *007*; 05MYKL015.2, *015*; 05MYKL031.1, *031*; 05MYKL045.1, *045*). Minor RFs (n = 4: 03MYKL018.1 *018*; 04MYKL016.1 *016*; 04MYKL019.1 *019*; 05MYKL043.1, *043*). Abbreviations of strain codes for minor RFs are shown in gray. C, Schematic representation of subtype structures of novel HIV-1 recombinants. Recombination breakpoints (sites I–IV) are indicated. Dotted vertical lines indicate the breakpoints (marked with asterisks) shared among Malaysian RFs. D, Neighbor-joining tree of eight near-full-length nucleotide sequences of novel Malaysian recombinants with reference sequences of HIV-1 group M subtypes and sub-subtypes (http://hiv-web.lanl.gov/). Selected HIV-1 genotypes of geographical importance are included: B′, Thai variant of subtype B; C_{IN}, Indian subtype C; C_{AF}, African subtype C; 01_{TH}, Thailand CRF01_AE; 01_{AF}, African CRF01_AE; 07, CRF07_BC; 08, CRF08_BC; 15, CRF15_01B, minor RF, minor recombinant form composed of CRF01_AE and subtype B. Branching orders were assessed by 100 bootstrap analyses, and values ≥70% are shown at the corresponding nodes of the tree. Scale bar represents 2% genetic distance (0.02 substitution/site).

epidemics between Thailand and Malaysia. In the early phase of the Malaysian epidemic, CRF01_AE and subtype B′ were circulating relatively independently among heterosexuals and IDUs, respectively, similar to the early stage of the Thai epidemic.[8,9] However, Tovanabutra and others recently reported that in a high-risk cohort in northern Thailand, CRF01_AE/B recombinants began to be identified in 2001 at 8.3% of incident cases and increased to 57.1% in 2002.[18] Due to the lack of availability of archival HIV specimens in the current study, we were not able to pinpoint the timing of emergence of CRF33_01B. However, the relatively long branch length of the CRF33_01B cluster (interstrain genetic diversity of 6.06 ± 0.50% (n = 4, isolates collected in 2005) compared with the interstrain genetic diversity of 3.10 ± 0.55% for Thailand CRF01_AE cluster (n = 4, isolates collected in 1990–1997) in near-full-length genomes) (Fig. 3D) suggests that the timing of the origin of CRF33_01B could be dated back to mid-1990s (unpublished data).

In summary, we report herein on a novel CRF that is circulating widely among various risk groups in Malaysia.

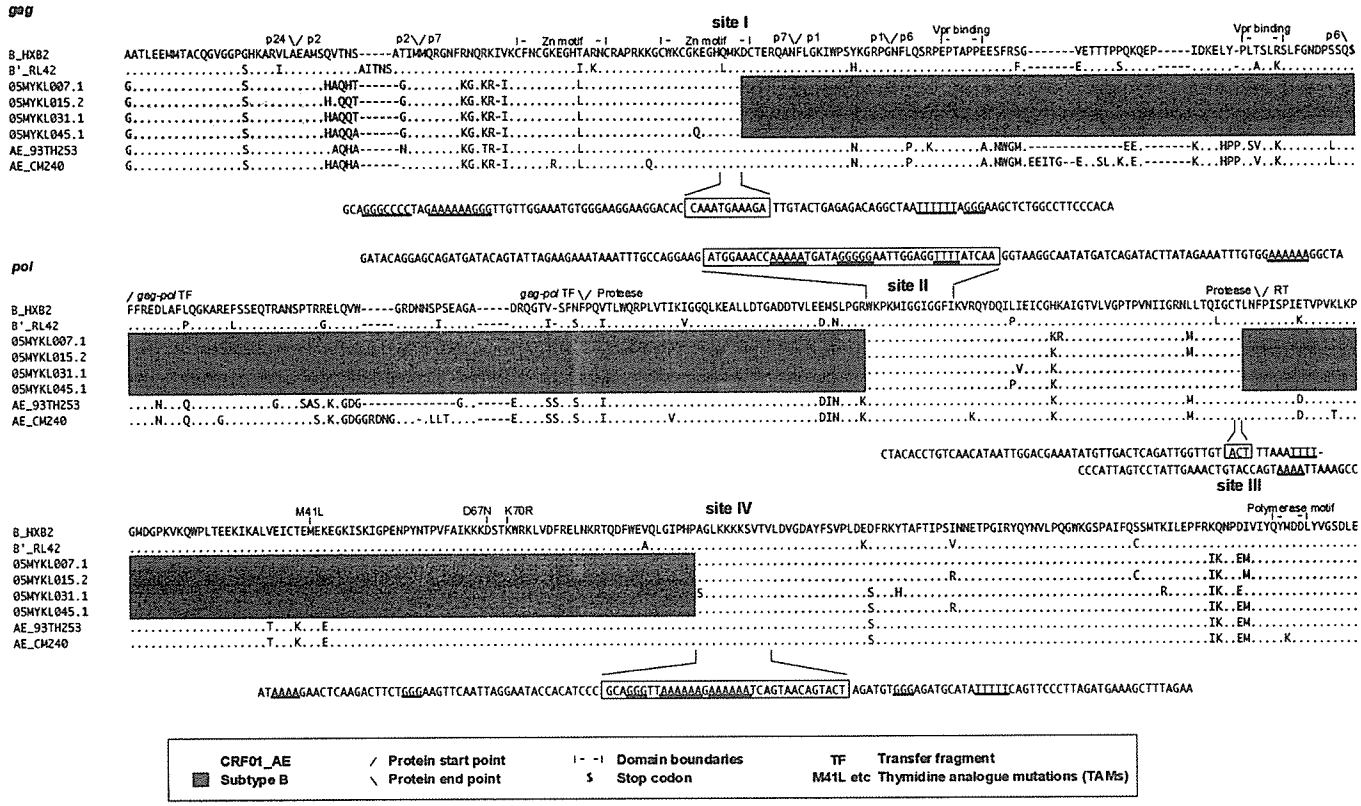

FIGURE 4. Sequence signatures in the vicinity of the recombination breakpoints in CRF33_01B. Amino acid sequence alignment of major recombinant form (RF) (CRF33_01B, n = 4) with subtype B (HXB2), B′ (RL42), and CRF01_AE (93TH253 and CM240) reference strains in *gag-pol* regions is shown. Four recombination breakpoints are clustered in this region. Periods (.) indicate the sequence identity with HXB2, and dashes (–) denote the gaps in the alignment. The CRF01_AE and subtype B regions are marked with different shadows. Unshaded areas are the presumed recombination breakpoints estimated by informative site analysis. Nucleotide sequences (consensus of four CRF33_01B isolates) within (boxed) and adjacent to (50-nucleotide region) the estimated recombination breakpoints (sites I–IV) are shown. Sequence landmarks in the Pro-RT region, including the boundaries of the domains of HIV-1 proteins, the conserved motifs, and the positions of major drug resistance mutations, are indicated at the top of the alignment.

Wide distribution of CRF33_01B involving all major ethnic and risk groups provides evidence for extensive bridging of HIV-1 transmission between different risk groups in Malaysia.

ACKNOWLEDGMENTS

We thank Kouichi Watanabe, Toshinari Onogi, Clarence Sim, and Margaret Lau for assistance; Brian Foley and Thomas Leitner for valuable advice on assignment of the new CRF; and Tim Mastro and Sai Kit Lam for critical reading of the manuscript. We also thank the patients for their participation in this study.

REFERENCES

1. Goh KL, Chua CT, Chiew IS, et al. The acquired immune deficiency syndrome: a report of the first case in Malaysia. *Med J Malaysia*. 1987;42: 58–60.
2. Joint United Nations Program on HIV/AIDS (UNAIDS). Available at: http://www.unaids.org. Accessed September 17, 2006.
3. Ministry of Health. *HIV/AIDS Report*, 2004.
4. UNAIDS. *AIDS Epidemic Update: December 2005*, 2005.
5. Malim MH, Emerman M. HIV-1 sequence variation: drift, shift, and attenuation. *Cell*. 2001;104:469–472.
6. Leitner T, Korber B, Daniels M, et al. HIV-1 subtype and circulating recombinant form (CRF) references sequences. In: Leitner T, Foley B, Hahn B, et al, eds. *HIV Sequence Compendium 2005*. Report no. LA-UR 06-0680. Los Alamos, NM: Theoretical Biology and Biophysics Group, Los Alamos National Library; 2005:41–48.
7. Robertson DL, Anderson JP, Bradac JA, et al. HIV-1 nomenclature proposal. *Science*. 2000;288:55–57.
8. Ou CY, Takebe Y, Weniger BG, et al. Independent introduction of two major HIV-1 genotypes into distinct high-risk populations in Thailand. *Lancet*. 1993;341:1171–1174.
9. Weniger BG, Takebe Y, Ou CY, et al. The molecular epidemiology of HIV in Asia. *AIDS*. 1994;8(Suppl 2):S13–S28.
10. Wasi C, Herring B, Raktham S, et al. Determination of HIV-1 subtypes in injecting drug users in Bangkok, Thailand, using peptide-binding enzyme immunoassay and heteroduplex mobility assay: evidence of increasing infection with HIV-1 subtype E. *AIDS*. 1995;9:843–849.
11. Vanichseni S, Kitayaporn D, Mastro TD, et al. Continued high HIV-1 incidence in a vaccine trial preparatory cohort of injection drug users in Bangkok, Thailand. *AIDS*. 2001;15:397–405.
12. Hudgens MG, Longini IM Jr, Vanichseni S, et al. Subtype-specific transmission probabilities for human immunodeficiency virus type 1 among injecting drug users in Bangkok, Thailand. *Am J Epidemiol*. 2002; 155:159–168.

13. Tovanabutra S, Polonis V, De Souza M, et al. First CRF01_AE/B recombinant of HIV-1 is found in Thailand. *AIDS*. 2001;15:1063–1065.
14. Viputtijul K, de Souza M, Trichavaroj R, et al. Heterosexually acquired CRF01_AE/B recombinant HIV type 1 found in Thailand. *AIDS Res Hum Retroviruses*. 2002;18:1235–1237.
15. Nguyen L, Hu DJ, Choopanya K, et al. Genetic analysis of incident HIV-1 strains among injection drug users in Bangkok: evidence for multiple transmission clusters during a period of high incidence. *J Acquir Immune Defic Syndr*. 2002;30:248–256.
16. Ramos A, Nguyen L, Hu DJ, et al. New HIV type 1 CRF01_AE/B recombinants displaying unique distribution of breakpoints from incident infections among injecting drug users in Thailand. *AIDS Res Hum Retroviruses*. 2003;19:667–674.
17. Swanson P, Devare SG, Hackett J Jr. Full-length sequence analysis of HIV-1 isolate CM237: a CRF01_AE/B intersubtype recombinant from Thailand. *AIDS Res Hum Retroviruses*. 2003;19:707–712.
18. Tovanabutra S, Beyrer C, Sakkhachornphop S, et al. The changing molecular epidemiology of HIV type 1 among northern Thai drug users, 1999 to 2002. *AIDS Res Hum Retroviruses*. 2004;20:465–475.
19. Tovanabutra S, Watanaveeradej V, Viputtikul K, et al. A new circulating recombinant form, CRF15_01B, reinforces the linkage between IDU and heterosexual epidemics in Thailand. *AIDS Res Hum Retroviruses*. 2003;19:561–567.
20. Brown TM, Robbins KE, Sinniah M, et al. HIV type 1 subtypes in Malaysia include B, C, and E. *AIDS Res Hum Retroviruses*. 1996;12:1655–1657.
21. Beyrer C, Vancott TC, Peng NK, et al. HIV type 1 subtypes in Malaysia, determined with serologic assays: 1992–1996. *AIDS Res Hum Retroviruses*. 1998;14:1687–1691.
22. Saraswathy TS, Ng KP, Sinniah M. Human immunodeficiency virus type 1 subtypes among Malaysian intravenous drug users. *Southeast Asian J Trop Med Public Health*. 2000;31:283–286.
23. Tee KK, Pon CK, Kamarulzaman A, et al. Emergence of HIV-1 CRF01_AE/B unique recombinant forms in Kuala Lumpur, Malaysia. *AIDS*. 2005;19:119–126.
24. Tee KK, Saw TL, Pon CK, et al. The evolving molecular epidemiology of HIV type 1 among injecting drug users (IDUs) in Malaysia. *AIDS Res Hum Retroviruses*. 2005;21:1046–1050.
25. Kato K, Sato H, Takebe Y. Role of naturally occurring basic amino acid substitutions in the human immunodeficiency virus type 1 subtype E envelope V3 loop on viral coreceptor usage and cell tropism. *J Virol*. 1999;73:5520–5526.
26. Salminen MO, Koch C, Sanders-Buell E, et al. Recovery of virtually full-length HIV-1 provirus of diverse subtypes from primary virus cultures using the polymerase chain reaction. *Virology*. 1995;213:80–86.
27. Yang R, Kusagawa S, Zhang C, et al. Identification and characterization of a new class of human immunodeficiency virus type 1 recombinants comprised of two circulating recombinant forms, CRF07_BC and CRF08_BC, in China. *J Virol*. 2003;77:685–695.
28. Rambaut A. *Se-Al (Sequence Alignment Editor)*, version 1.0, alpha 1. Oxford, England: University of Oxford, Department of Zoology; 1996.
29. Saitou N, Nei M. The neighbor-joining method: a new method for reconstructing phylogenetic trees. *Mol Biol Evol*. 1987;4:406–425.
30. Kimura M. A simple method for estimating evolutionary rates of base substitutions through comparative studies of nucleotide sequences. *J Mol Evol*. 1980;16:111–120.
31. Lole KS, Bollinger RC, Paranjape RS, et al. Full-length human immunodeficiency virus type 1 genomes from subtype C-infected seroconverters in India, with evidence of intersubtype recombination. *J Virol*. 1999;73:152–160.
32. Klarmann GJ, Schauber CA, Preston BD. Template-directed pausing of DNA synthesis by HIV-1 reverse transcriptase during polymerization of HIV-1 sequences in vitro. *J Biol Chem*. 1993;268:9793–9802.
33. Quinones-Mateu ME, Gao Y, Ball SC, et al. In vitro intersubtype recombinants of human immunodeficiency virus type 1: comparison to recent and circulating in vivo recombinant forms. *J Virol*. 2002;76:9600–9613.

THE JOURNAL OF BIOLOGICAL CHEMISTRY VOL. 281, NO. 18, pp. 12688–12698, May 5, 2006
Printed in the U.S.A.

Structural and Molecular Interactions of CCR5 Inhibitors with CCR5*

Received for publication, November 28, 2005, and in revised form, January 25, 2006 Published, JBC Papers in Press, February 23, 2006, DOI 10.1074/jbc.M512688200

Kenji Maeda[‡§¶], Debananda Das[¶], Hiromi Ogata-Aoki[‡§], Hirotomo Nakata[‡§], Toshikazu Miyakawa[§], Yasushi Tojo[‡§], Rachael Norman[¶], Yoshikazu Takaoka[‖], Jianping Ding[**], Gail F. Arnold[**], Eddy Arnold[**], and Hiroaki Mitsuya[‡§¶1]

From the [‡]Department of Hematology and [§]Department of Infectious Diseases, Kumamoto University Graduate School of Medical and Pharmaceutical Sciences, Kumamoto 860-8556, Japan, the [¶]Experimental Retrovirology Section, HIV and AIDS Malignancy Branch, NCI, National Institutes of Health, Bethesda, Maryland 20892, the [‖]Minase Research Institute, Ono Pharmaceutical Co. Ltd., Osaka 618-8585, Japan, and the [**]Center for Advanced Biotechnology and Medicine, and Chemistry and Chemical Biology Department, Rutgers University, Piscataway, New Jersey 08854

We have characterized the structural and molecular interactions of CC-chemokine receptor 5 (CCR5) with three CCR5 inhibitors active against R5 human immunodeficiency virus type 1 (HIV-1) including the potent *in vitro* and *in vivo* CCR5 inhibitor aplaviroc (AVC). The data obtained with saturation binding assays and structural analyses delineated the key interactions responsible for the binding of CCR5 inhibitors with CCR5 and illustrated that their binding site is located in a predominantly lipophilic pocket in the interface of extracellular loops and within the upper transmembrane (TM) domain of CCR5. Mutations in the CCR5 binding sites of AVC decreased gp120 binding to CCR5 and the susceptibility to HIV-1 infection, although mutations in TM4 and TM5 that also decreased gp120 binding and HIV-1 infectivity had less effects on the binding of CC-chemokines, suggesting that CCR5 inhibition targeting appropriate regions might render the inhibition highly HIV-1-specific while preserving the CC chemokine-CCR5 interactions. The present data delineating residue by residue interactions of CCR5 with CCR5 inhibitors should not only help design more potent and more HIV-1-specific CCR5 inhibitors, but also give new insights into the dynamics of CC-chemokine-CCR5 interactions and the mechanisms of CCR5 involvement in the process of cellular entry of HIV-1.

Highly active antiretroviral therapy has brought about a major impact on the acquired immunodeficiency syndrome (AIDS) epidemics in industrially advanced nations (1, 2), however, eradication of HIV-1[2] appears to be currently impossible mainly because of the viral reservoirs remaining in blood and infected tissues (3). Successful antiviral drugs, in theory, exert their virus-specific effects by interacting with viral components such as viral genes or their transcripts without disturbing cellular metabolisms or functions (2). However, at present, no antiretroviral drugs or agents have been demonstrated to be completely specific for HIV-1 and devoid of toxicity or side effects in the therapy of AIDS (4). Limitations of antiviral therapy of AIDS are exacerbated by complicated regimens, emergence of drug-resistant HIV-1 variants (1), and a number of inherent adverse effects (5).

Thus, identification of new antiretroviral drugs that have unique mechanisms of action and produce no or least minimal side effects remains an important therapeutic objective (2, 4). CCR5 is a member of the G protein-coupled, seven-transmembrane segment receptors, which comprise the largest superfamily of proteins in the body (6). In 1996, it was revealed that CCR5 serves as one of the two essential coreceptors for HIV-1 entry to human $CD4^+$ cells, thereby serving as an attractive target for possible intervention of HIV-1 infection (7–10). Aplaviroc (AVC; AK602/ONO4128/873140; Fig. 1), a novel spirodiketopiperazine derivative, represents a CCR5 inhibitor that specifically binds to human CCR5 with a high affinity, greatly blocks HIV-1-gp120/CCR5 binding, and exerts potent activity against a wide spectrum of laboratory and primary R5-HIV-1 isolates including multidrug-resistant $HIV\text{-}1_{MDR}$ (IC_{50} values of 0.2–0.6 nM) (11). AVC, despite its much greater anti-HIV-1 activity than other previously published CCR5 inhibitors including TAK-779 and SCH-C (Fig. 1), preserves RANTES and macrophage inflammatory protein-1β binding to $CCR5^+$ cells and their functions, whereas TAK-779 and SCH-C fully block the CC-chemokines/CCR5 interactions (11). AVC reportedly has an extensive and prolonged CCR5 occupancy as examined in phytohemagglutinin-activated peripheral blood mononuclear cells ($t_{1/2} \sim 9$ h) (12) and in circulating lymphocytes in HIV-1-negative and HIV-1-positive individuals ($t_{1/2}$ of 69–152 h depending on different AVC doses) (37). In a randomized, placebo-controlled short-term monotherapy trial in patients with AIDS including those who were drug-experienced, AVC demonstrated potent antiretroviral activity and brought about significant reduction in HIV-1 viremia (by ~1.7 log) in AIDS patients (38).

In the present study, we examined the profile of binding to and interactions with CCR5 of three CCR5 inhibitors, AVC, SCH-C, and TAK-779. We also conducted structural analyses of the interactions of CCR5 inhibitors with CCR5, using homology modeling, robust structure refinement, and docking. Notably, the molecular modeling analyses were combined and fine-tuned with the results of the saturation binding assay using a panel of mutant CCR5-expressing cells and [^{3}H]CCR5 inhibitors and the resultant configurations and orientations of inhibitors docked within the hydrophobic cavity of CCR5 yielded structure-activity predictions and interpretations consistent with the observed experimental data. The present approach of combining the site-directed mutagenesis-based data and molecular modeling should represent a

* This work was supported in part by the Intramural Research Program of the Center for Cancer Research, NCI, National Institutes of Health, and in part by a grant-in-aid for Scientific Research (Priority Areas) from the Ministry of Education, Culture, Sports, Science, and Technology of Japan (Monbu-Kagakusho), a Grant for Promotion of AIDS Research from the Ministry of Health, Welfare, and Labor of Japan Kosei Rohdosho H15-AIDS-001, and the Cooperative Research Project on Clinical and Epidemiological Studies of Emerging and Re-emerging Infectious Diseases (Renkei Jigyo number 78, Kumamoto University) of Monbu-Kagakusho. The costs of publication of this article were defrayed in part by the payment of page charges. This article must therefore be hereby marked "*advertisement*" in accordance with 18 U.S.C. Section 1734 solely to indicate this fact.

[1] To whom correspondence should be addressed. Tel.: 81-96-373-5156; Fax: 81-96-363-5265; E-mail: hmitsuya@helix.nih.gov.

[2] The abbreviations used are: HIV-1, human immunodeficiency virus, type 1; AVC, aplaviroc; CCR5, CC-chemokine receptor 5; MIP-1α, macrophage inflammatory protein-1α; RANTES, regulated upon activation, normal T cell expressed and secreted; CHO, Chinese hamster ovary; FCS, fetal calf serum; mAb, monoclonal antibody; TM, transmembrane; gp, glycoprotein.

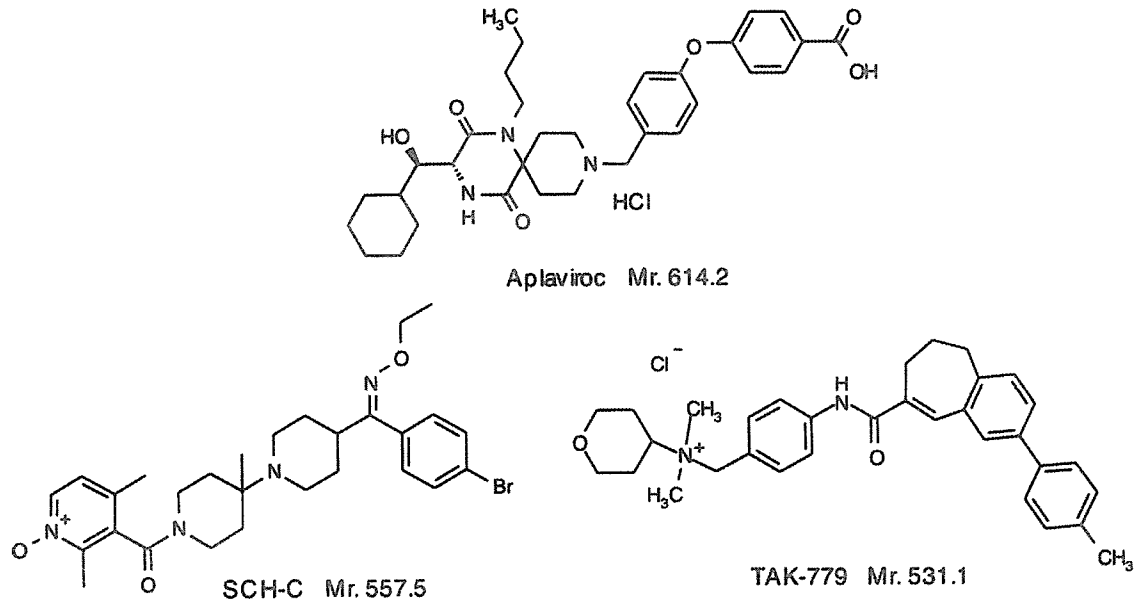

FIGURE 1. **Structures of AVC, TAK-779, and SCH-C.**

valuable strategy for gaining structural insights for membrane-bound proteins for which x-ray crystal structures are not as yet available. The present data delineating residue by residue interactions of CCR5 with CCR5 inhibitors should not only help design more potent and more HIV-1-specific CCR5 inhibitors, but also give new insights into the dynamics of CC-chemokine-CCR5 interactions and the mechanisms of CCR5 involvement in the process of cellular entry of HIV-1.

EXPERIMENTAL PROCEDURES

Reagents—A CCR5 inhibitor, AVC, was designed and synthesized as previously published (11). Two other CCR5 inhibitors, TAK-779 and SCH-351125 (SCH-C), were synthesized based on the previously published structures (13, 14) (Fig. 1). These three CCR5 inhibitors were tritiated by reductive amination with sodium triacetoxyborotritide (15), methylation with [^{3}H]methyliodide, and/or heterogeneous catalytic exchange with tritium gas (16). Two ^{125}I-labeled chemokines (macrophage inflammatory protein-1α (MIP-1α) and regulated upon activation, normal T cell expressed and secreted (RANTES)) were purchased from Amersham Biosciences and ^{125}I-labeled macrophage inflammatory protein-1β (MIP-1β) was purchased from PerkinElmer Life Sciences, Inc. Their corresponding unlabeled chemokines were purchased from PeproTech Inc. (Rocky Hill, NJ). Recombinant HIV-1_{YU2} gp120 (rgp120) and human soluble CD4 (sCD4) were purchased from Immuno Diagnostics, Inc. (Woburn, MA).

Cells and Viruses—The Chinese hamster ovary (CHO) cells overexpressing CCR5 (17) were maintained in Ham's F-12 medium (Invitrogen) supplemented with 10% fetal calf serum (FCS: JRH Biosciences, Lenaza, KS) and 50 units/ml penicillin and 50 μg/ml streptomycin in the presence of 5 μg/ml blasticidin S hydrochloride. The HeLa-CD4-LTR-β-galactosidase indicator cell line expressing human CCR5 (CCR5$^+$MAGI (multinuclear activation of galactosidase indicator) cells) (18) was a kind gift from Dr. Yosuke Maeda, Kumamoto University Graduate School of Medical and Pharmaceutical Sciences, Japan. CCR5$^+$MAGI cells were maintained in Dulbecco's modified Eagle's medium (DMEM) supplemented with 10% FCS, 200 μg/ml G418, 100 μg/ml hygromycin B, and 100 μg/ml zeomycin. The U373-MAGI cell line was obtained from the AIDS Research and Reference Reagent Program, NIAID, National Institutes of Health (Bethesda, MD). U373-MAGI cells were maintained in Dulbecco's modified Eagle's medium supplemented with 10% FCS, 200 μg/ml G418, and 100 μg/ml hygromycin B. An R5-HIV-1 strain, HIV-1_{BaL}, was employed for the determination of the susceptibility of mutant CCR5 ($CCR5_{MT}$)-expressing cells to the infectivity of HIV-1.

Generation of Wild-type and $CCR5_{MT}$-overexpressing Cells—A mammalian expression vector pZeoSV2 (Invitrogen) carrying the human wild-type *CCR5* ($CCR5_{WT}$) gene (pZeoSV-*CCR5*) (18) was a kind gift from Dr. Yosuke Maeda. A variety of plasmids carrying a mutant *CCR5*-encoding gene were generated using the site-directed mutagenesis technique employing the QuikChange site-directed mutagenesis kit (Stratagene, La Jolla, CA) as described by the manufacturer. Mutations introduced into the *CCR5* gene were introduced through: (i) substitution of an amino acid(s) or (ii) deletion of an amino acid(s) at selected amino acid positions of CCR5. A mutation from Gly to Arg at position 163, where the corresponding amino acid in simian CCR5 is Arg, was also introduced. This G163R substitution has been reported to reduce the binding of R5-HIV-1-gp120 to human CCR5 and the susceptibility to HIV-1 (19). All these plasmids were confirmed to contain only the desired mutation(s) by nucleotide sequencing.

CHO cells (or U373-MAGI cells) were transfected with a plasmid containing the $CCR5_{WT}$-encoding gene or a plasmid carrying a $CCR5_{MT}$-encoding gene using Lipofectamine (Invitrogen); the transfectants were magnetically sorted, following treatment with an anti-CCR5 monoclonal antibody (2D7 or 3A9; BD Pharmingen, San Diego, CA), using Dynabeads M-450 coupled to goat anti-mouse IgG (Dynal A.S., Oslo, Norway); and the cells were cloned using the limiting dilution technique.

Determination of CCR5 Expression Levels in CHO and U373-MAGI Cells—CCR5 expression levels of the various clones described above were determined using three indicators: (i) maximal amounts of [^{3}H]AVC bound to cells (B_{max}); (ii) mean florescence intensity values when stained with monoclonal antibody (mAb) 3A9; and (iii) mean florescence intensity values when stained with mAb 2D7. The antigenic epitope for 2D7 is located distant from that for 3A9 (20) and 3A9 does not compete with AVC binding to CCR5 (data not shown). The expression levels were expressed as % control ($CCR5_{WT}$-expressing cells as control), and the highest value obtained was chosen as the estimated

CCR5 expression level. There were no clones that had low values in all three indicators, thus sustaining that the current method used for the CCR5 expression levels was thought to be legitimate. CD4 and CCR5 expression levels were also determined using the quantitative fluorescence-activated cell sorting assay system (Quantum Simply Cellular Kit; Sigma) using 3A9 and 2D7 (12). For the HIV-1 susceptibility assay, U373-MAGI clones that expressed CD4 molecules ranging 10–25 × 10^4 antigen-binding sites were selected. $CCR5_{MT}$-expressing CHO cells were maintained in Ham's F-12 medium containing 10% FCS and 100 μg/ml zeomycin. $CCR5_{WT}$- and $CCR5_{MT}$-expressing U373-MAGI cells were cultured in Dulbecco's modified Eagle's medium supplemented with 10% FCS, 200 μg/ml G418, 100 μg/ml hygromycin B, and 100 μg/ml zeomycin.

Saturation Binding Assay Using ^{3}H-Labeled CCR5 Inhibitors—Saturation binding assay using ^{3}H-labeled CCR5 inhibitors was conducted and the K_D values of CCR5 inhibitors in $CCR5_{WT}$-, or $CCR5_{MT}$-expressing CHO cells were calculated as previously described (11).

Radiolabeled Inhibitor Binding/Competition Studies—$CCR5_{WT}$-expressing cells (1.5 × 10^5) were plated onto 48-well microculture plates, incubated for 24 h, rinsed, exposed to [^{3}H]AVC, [^{3}H]SCH-C, or [^{3}H]TAK-779 for 15 min at room temperature, subsequently exposed to various concentrations of unlabeled CCR5 inhibitors, incubated for 30 min, thoroughly washed, lysed, and the radioactivity in the lysates was counted. All experiments were performed in duplicate. The amounts of each ^{3}H-labeled CCR5 inhibitor bound to the cells are shown as mean % control values. Standard deviation values are indicated with the vertical lines. To obtain control values, the experiment was also performed without the addition of unlabeled CCR5 inhibitors.

Determination of CC-chemokine- and HIV-1 Gp120 Binding Affinity to $CCR5_{WT}$ and $CCR5_{MT}$—Binding profiles of chemokines to $CCR5_{WT}$- or $CCR5_{MT}$-expressing cells were determined using ^{125}I-labeled chemokines as previously reported (11) with minor modifications. In brief, $CCR5_{WT}$- or $CCR5_{MT}$-expressing cells (1.5 × 10^5) were plated onto 48-well microculture plates, incubated for 24 h, rinsed, exposed to 5 nM ^{125}I-MIP-1α, ^{125}I-MIP-1β, or ^{125}I-RANTES at room temperature for 1 h, thoroughly washed with phosphate-buffered saline, lysed with 0.5 ml of 1 N NaOH, and the radioactivity in the lysates counted. The nonspecific binding of the labeled chemokine to the cells was determined based on the radioactivity detected in the wells plated with the same number of CCR5-negative CHO (CHO-K1) cells exposed to an equal amount of ^{125}I-labeled chemokine. Determination of the binding profiles of HIV-1-rgp120 to $CCR5_{WT}$ or $CCR5_{MT}$ was also conducted. Briefly, $CCR5^+$CHO cells were exposed to rgp120 (5 μg/ml) and sCD4 (5 μg/ml: biotinylated using EZ-link sulfo-NHS-SS-biotin (Pierce)) for 1 h at 37 °C. Cells were washed and binding of the rgp120-sCD4 complex to $CCR5^+$CHO cells was determined using phycoerythrin-conjugated streptavidin (SA-PE: BD Pharmingen). Nonspecific binding was determined based on the mean florescence intensity of SA-PE with sCD4 but without rgp120. Because CCR5 expression levels vary among CCR5 clones, the % binding (occupancy) values for ^{125}I-chemokines and rgp120 were normalized using the following formula: % binding (occupancy) = 100 × (amount of ^{125}I-chemokine or rgp120 bound to $CCR5_{MT}$/amount of ^{125}I-chemokine or rgp120 bound to $CCR5_{WT}$) × (number of $CCR5_{WT}$/number of $CCR5_{MT}$), where numbers of $CCR5_{WT}$ and $CCR5_{MT}$ are expressed as B_{max} (cpm) or mean florescence intensity values as described above.

Determination of HIV-1 Susceptibility of $CCR5_{WT}$- and $CCR5_{MT}$-expressing Cells—The susceptibility of $CCR5_{WT}$- and $CCR5_{MT}$-expressing cells to the infection by an R5-HIV-1 strain, $HIV\text{-}1_{BaL}$, was determined as previously described (22). In brief, target cells ($CCR5_{WT}$- or $CCR5_{MT}$-expressing U373-MAGI cells; 10^4/well) were plated onto 96-well flat microtiter culture plates, inoculated with 100 $TCID_{50}$ of $HIV\text{-}1_{BaL}$ on the following day, cultured for 48–72 h, stained with 400 μg/ml of 5-bromo-4-chloro-3-indolyl-β-D-galactopyranoside (X-gal), and all blue cells were counted. All experiments were performed in triplicate. For testing each $CCR5_{MT}$-expressing cell preparation, multiple (5 to 13) clones were examined. In each set of experiments, $CCR5_{WT}$-clone 1 was included and served as a standard. Percent infection in $CCR5_{WT}$- and $CCR5_{MT}$-expressing cells was determined using the following formula: % Infection = 100 × (mean blue cell number in a well)/(mean blue cell number in a well of $CCR5_{WT}$-clone 1).

Structural Modeling of the Interactions of CCR5 Inhibitors with Wild-type and Mutant CCR5 Species—An initial structural model of CCR5 was defined with homology modeling using the crystal structure of bovine rhodopsin as a template (23). This resulted in the initial placement of the helices and side chains. The CCR5-inhibitor complex structures were defined with an iterative optimization of CCR5 and inhibitor structures in the presence of each other, using software tools from Schrödinger (Schrödinger, LLC, New York), as described below. The conformational flexibility of both CCR5 and the inhibitors were taken into account. The molecular structures of AVC, SCH-C, and TAK-779, without the presence of counter-ions and solvents, were obtained by minimization using the MMFF94 force field (24). For each minimized inhibitor configuration, a set of low energy structures was generated by performing a Monte Carlo sampling of their conformations. Thus obtained structures were used as starting structures for docking calculations where their conformations were further refined.

The protonation states of CCR5 residues were assigned, and residues more than 20 Å from the active site were neutralized. In an attempt to place an inhibitor within CCR5, initially the active site was artificially enlarged by mutating Tyr^{108}, Cys^{178}, Glu^{283}, and Met^{287} to Ala. The van der Waals radii of inhibitor atoms were scaled by a factor of 0.70 to reduce steric clashes and docked into CCR5. After obtaining an initial set of CCR5-inhibitor complexes, residues 108, 178, 283, and 287 were mutated back from Ala to their original states. CCR5 atoms within 15 Å of an initially placed inhibitor were subsequently refined. It was achieved by using the rotamer library of Xiang and Honig (25) and optimizing each side chain one at a time holding all other side chains fixed. After convergence, all side chains were simultaneously energy minimized using the OPLS-AA force field (26) to remove any remaining clashes. The inhibitors were docked again and scored to estimate their relative affinity. The docked complexes with higher scores were visually examined along with the mutational data to select the best possible CCR5-inhibitor complex.

Mutated CCR5 structures were defined using the wild-type CCR5 structure and optimized using the OPLS2003 force field. Charges were taken from the force field. The minimization was carried out until the gradient was below 0.2 kJ/Å-mol. Resulting minimized structures were used as starting structures for obtaining docked complexes of mutated CCR5 with inhibitors using the protocol described above. Visualization, structural refinement, and docking were performed using Maestro 7.0, MacroModel 9.0, Prime 1.2, Glide 3.5, and IFD script from Schrödinger, LLC (New York). The extra precision mode of Glide, which has higher penalties for unfavorable and unphysical interactions, was used (27). Computations were carried out on a multiprocessor SGI Origin 3400 computer platform.

A probe radius of 1.4 Å with Connolly surfaces generated was used to define binding site cavities using the method of Exner *et al.* (28) as implemented in the MOLCAD tool in Sybyl 7.0 (Tripos, Inc., St. Louis,

TABLE 1
Binding affinity of CCR5 inhibitors to mutant CCR5s

Mutant CCR5 overexpressed on CHO cells		K_D value[a]			Gp120/sCD4 binding[b]
		Aplaviroc	SCH-C	TAK-779	
		nM			% control
Wild type		2.9 ± 1.0	16.0 ± 1.5	30.2 ± 7.6	100 ± 13.3
D11A	NH_2 terminus	3.0 ± 0.6	12.4 ± 2.0	24.5 ± 3.7	35.4 ± 4.7
Y37A	TM1	7.9 ± 0.9	>200	**98.9 ± 11.5**	35.4 ± 3.7
Y108A		**19.8 ± 4.4**[c]	11.8 ± 1.1	>200	13.2 ± 1.0
F112L		4.0 ± 2.6	30.0 ± 6.4	33.0 ± 7.2	
F112Y	TM3	6.8 ± 1.1	35.8 ± 7.6	28.5 ± 3.1	111 ± 6.9
F113A		**13.3 ± 2.3**	43.8 ± 6.3	32.7 ± 3.3	
F113Y		8.6 ± 3.4	45.3 ± 12.1	32.4 ± 3.0	
G163A	TM4-ECL2[d]	8.0 ± 4.2	25.0 ± 8.2	24.0 ± 5.9	
G163R		>200	46.3 ± 16.5	88.3 ± 22.9	34.1 ± 5.4
R168A		**13.2 ± 3.3**	21.0 ± 8.1	43.0 ± 4.7	
K171A/E172A		2.8 ± 0.1	34.8 ± 6.8	30.5 ± 0.7	29.6 ± 2.2
C178A		>200	27.1 ± 4.4	34.5 ± 3.5	20.9 ± 1.0
S180A		5.7 ± 1.2	31.8 ± 14.4	18.2 ± 3.2	
S180T	ECL2	1.5 ± 0.6	25.4 ± 6.8	41.0 ± 3.8	101 ± 15.0
S180E		**13.9 ± 1.7**	16.5 ± 2.2	25.0 ± 3.5	51.6 ± 1.1
Y184A/S185A		2.0 ± 0.8	21.3 ± 5.0	28.0 ± 2.5	
Y184A/S185A/Q186A/Y187A		2.0 ± 0.6	14.9 ± 0.6	32.3 ± 5.8	
Q186A/Y187A		2.8 ± 0.5	14.7 ± 8.8	35.2 ± 5.8	
Q188A		6.6 ± 1.4	23.8 ± 1.5	37.9 ± 2.5	
WKNF190del		>200	**49.2 ± 1.7**	80.1 ± 16.7	
K191A		>200	26.5 ± 7.1	35.0 ± 3.8	45.7 ± 0.6
K191R	ECL2-TM5	**9.0 ± 5.6**	34.1 ± 19.1	47.1 ± 8.8	
K191N		**14.2 ± 1.1**	35.8 ± 9.2	35.1 ± 9.3	
K197A	TM5	**9.2 ± 4.3**	16.8 ± 2.9	14.7 ± 1.1	
I198A		**24.6 ± 4.8**	**52.4 ± 3.0**	54.9 ± 6.9	51.7 ± 3.0
Y251A	TM6	**36.5 ± 9.5**	21.5 ± 8.6	43.0 ± 4.5	14.5 ± 0.7
E283A		>200	>200	>200	4.3 ± 0.6
M287A	TM7	6.8 ± 2.3	28.0 ± 9.1	39.8 ± 7.5	104 ± 3.9
M287E		**14.8 ± 1.7**	32.2 ± 4.2	53.1 ± 3.7	22.0 ± 0.8

[a] K_D values were determined using saturation binding assays ("Experimental Procedures").
[b] Gp120/sCD4 binding affinity to $CCR5_{MT}$ is shown by % control (see "Experimental Procedures" for reference); the data are also shown in Fig. 8A.
[c] K_D values more than 3-fold compared to that with $CCR5_{WT}$ are shown in bold. All K_D values were determined on multiple occasions (twice to 6 times). Considering the standard deviation for the wild type and other mutations, a 3-fold difference was seen to be statistically significant.
[d] ECL, extracellular loop.

MO). Lipophilic potential was mapped onto the cavities using parameters from Viswanadhan *et al.* (29).

RESULTS

Site-directed Mutagenesis of CCR5 and Binding Affinity of CCR5 Inhibitors—We have previously reported (11) that AVC competitively blocked the binding of a monoclonal antibody, 45531, which is known to be specific against the C-terminal half (or domain B) of the second extracellular loop (ECL2B) of CCR5 (21), whereas AVC failed to block or only partially blocked the binding of two other monoclonal antibodies, 2D7 and 45523, specific for CCR5 but not for its ECL2B. When we examined three additional monoclonal antibodies, 3A9 and 45502 (both specific for NH_2 terminus) and 45549 (multidomain reactive) (20, 21), none of these antibodies were replaced by AVC (data not shown). These data suggest that the potent inhibitory activity of AVC against R5 HIV-1 infection stems from its binding to ECL2B and/or its vicinity with high affinity.

In an attempt to delineate the CCR5 binding profile of the three CCR5 inhibitors, we generated a variety of CCR5 mutant-overexpressing ($CCR5_{MT}$) CHO cells and determined the K_D values of each inhibitor to mutant CCR5 species using the saturation binding assay with tritiated inhibitors. When we determined the K_D value of AVC with respect to a CCR5 mutant carrying an Asp to Ala substitution at position 11 of the amino terminus domain ($CCR5_{D11A}$), the value was 3.0 nM, virtually identical to the K_D value with wild-type CCR5 ($CCR5_{WT}$; Table 1), indicating that the D11A substitution did not affect the binding of AVC to CCR5. The K_D value of AVC with respect to $CCR5_{Y37A}$ was moderately greater with 7.9 nM (2.7-fold compared with the K_D value with regard to $CCR5_{WT}$). On the other hand, those of TAK-779 and SCH-C to $CCR5_{Y37A}$ were 98.9 nM (3.3-fold compared with the K_D with regard to $CCR5_{WT}$) and >200 nM (>12.5-fold), respectively, in agreement with the previous reports in which both TAK-779 and SCH-C apparently failed to bind, probably explaining that these inhibitors failed to block HIV-1 infection of $CCR5_{Y37A}$-expressing cells (30, 31). These data suggest that the binding of TAK-779 and SCH-C to $CCR5_{WT}$ is more dependent on interactions with Tyr37 than that of AVC. We also generated a series of CCR5-overexpressing CHO cells carrying a mutation(s) at a selected amino acid position(s). As shown in Table 1, the mutations that substantially (more than 3-fold compared with AVC binding to $CCR5_{WT}$) affected the K_D values of AVC were as follows: Y108A and F113A in the third transmembrane domain (TM3) of CCR5; R168A and S180E in ECL2; K191R and K191N of the interface of ECL2B and TM5; K197A and I198A of TM5; Y251A of TM6; and M287E of TM7. The mutations that greatly diminished the binding of AVC (values of >200 nM) to CCR5 were as follows: G163R, C178A, WKNF190del, K191A, and E283A. It is worthwhile to interject that Lys^{191} in ECL2 is reported to be critical for the binding of RANTES, MIP-1α, and MIP-1β to CCR5 (32, 33), whereas Cys^{178} is presumed to form a disulfide bond with Cys^{101} of ECL1 and to be critical for the conformation of CCR5 (34). Mutations that substantially affected the binding of TAK-779 and SCH-C to CCR5 were as follows: Y37A, Y108A, and E283A for TAK-779; and Y37A, WKNF190del, I198A, and E283A for SCH-C. It is noteworthy that the number of mutations that affected the binding of AVC was notably greater than those of TAK-779 and SCH-C. Thus, the CCR5 binding modes of AVC, TAK-779, and SCH-C apparently share some similar features but also have some distinct differences.

Interactions of CCR5 Inhibitors with CCR5

Structural Analysis Locates Aplaviroc in the Interface of ECL and TM Domains—In the present study, a three-dimensional model of human CCR5-CCR5 inhibitor complex was defined by combining the results of site-directed mutagenesis-based analyses (Table 1) and molecular modeling that involved structure refinement and simultaneous docking of inhibitors to an initial structure of CCR5 based on the crystal structure of bovine rhodopsin (23). Fig. 2 illustrates the three-dimensional model of CCR5 that has a seven-transmembrane helical structure. Six hydrophobic cavities were identified in the extracellular, transmembrane, and intracellular domains of CCR5. Among them, a hydrophobic cavity to which CCR5 inhibitors highly likely to bind was identified based on its size and location (*red arrowhead* in Fig. 2). This cavity is the largest one among the six that can accommodate a molecule of the size of AVC and other CCR5 inhibitors and is in the region implicated to have the greatest effect on K_D values with amino acid substitutions introduced in CCR5 among the six hydrophobic cavities identified. It should be noted, however, that the conformations of CCR5 without an inhibitor and CCR5 with the inhibitor can be substantially different from each other, because significant conformational changes would be expected to follow ligand binding to CCR5. Nevertheless, it is intriguing to note that this largest cavity corresponds to the binding site for the retinal ligand in bovine rhodopsin; given the propensity of this pocket to bind fairly large ligands such as the CCR5 inhibitors, it is possible that this binding cavity could accommodate some as-yet uncharacterized ligands produced in the body during the normal function of CCR5, potentially even some with regulatory roles.

FIGURE 2. **Hydrophobic cavities identified within CCR5.** Six hydrophobic cavities are identified within human CCR5, defined using MOLCAD (Sybyl 7.0). Note the largest hydrophobic cavity (*red arrowhead*) that is likely to accommodate a molecule of the size of AVC and other CCR5 inhibitors and is in the region implicated to have greatest effects on K_D values (see mutagenesis-based results in Table 1).

Based on the set of the K_D values of AVC in relation to various mutant CCR5 species overexpressed on CHO cells (Table 1), structural analysis of AVC-CCR5 interactions was conducted, which suggested that a series of intramolecular and intermolecular hydrogen bonds occur, which should stabilize the CCR5-AVC complex. We identified a significant network of hydrogen bonds among four amino acid residues: Gly^{163}, Ser^{180}, Lys^{191}, and Thr^{195} (Fig. 3*A*). Gly^{163} is located in TM4, Ser^{180} in ECL2, and Lys^{191} and Thr^{195} in TM5. Another network of hydrogen bonds was identified among another four amino acid residues: Tyr^{37}, Glu^{283}, Met^{287}, and Tyr^{108} (Fig. 3*B*). Tyr^{37} is located in TM1, Tyr^{108} in TM3, and Glu^{283} and Met^{287} in TM7. These hydrogen bond networks spanning multiple domains appear to maintain the optimal shape of the cavity for the binding of AVC. Indeed, further analysis of the cavity also revealed that the ECL regions have some hydrophilic characters (Fig. 4*A*, *red arrowhead*), whereas the rest of the cavity is mostly lipophilic (Fig. 4*A*). The carboxyl and hydroxymethyl of AVC interact with the hydrophilic regions of CCR5. The rest of AVC inter-

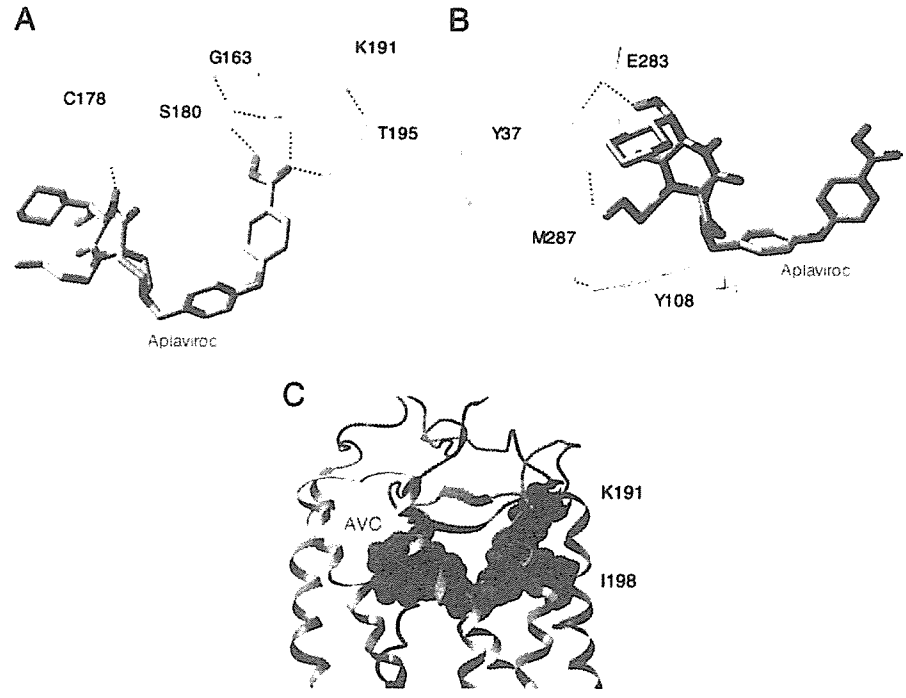

FIGURE 3. **Hydrogen bond networks within CCR5 critical for AVC binding to CCR5.** The structure of the CCR5-AVC complex was defined with iterative structural refinement using docking and homology modeling. Only polar hydrogen atoms are shown. *Panel A*, an intramolecular hydrogen bond network comprised of Gly^{163}, Ser^{180}, Lys^{191}, and Thr^{195} is seen. Gly^{163} is located in TM4, Ser^{180} in ECL2, and Lys^{191} and Thr^{195} in TM5. The structural analyses illustrate the presence of intermolecular hydrogen bonds of AVC with residues Cys^{178}, Ser^{180}, Lys^{191}, and Thr^{195} of CCR5. *Panel B*, an intramolecular hydrogen bond network is seen involving Tyr^{37}, Glu^{283}, Met^{287}, and Tyr^{108}. Tyr^{37} is located in TM1, Tyr^{108} in TM3, and Glu^{283} and Met^{287} in TM7. Glu^{283} forms hydrogen bond interactions with the hydroxymethyl of AVC. Intramolecular hydrogen bonds are shown in *pink*, and the intermolecular hydrogen bonds in *green*. Note that the hydrogen bond networks spanning multiple domains should maintain the optimal shape of the cavity for the binding of AVC (Fig. 4, *A* and *B*). *Panel C*, the predicted van der Waals contact between AVC and CCR5 residues Lys^{191} and Ile^{198}. AVC is shown in *green spheres*, whereas Lys^{191} and Ile^{198} in *magenta*.

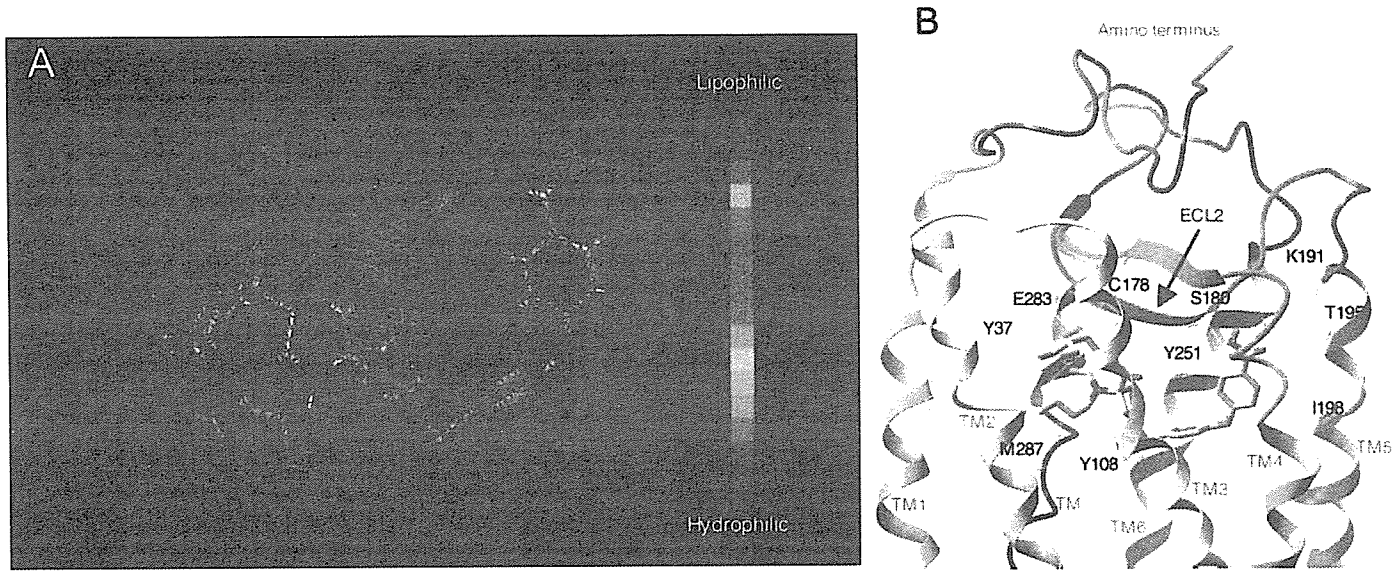

FIGURE 4. **The configuration of aplaviroc within CCR5.** *Panel A*, AVC lodged within the binding cavity of CCR5. The CCR5 cavity was defined with its lipophilic potential using MOLCAD. The region near the extracellular domain has some hydrophilic character (*red arrowhead*), whereas the rest of the cavity is mostly lipophilic. The carboxyl and hydroxymethyl of AVC interact with the hydrophilic regions of CCR5, whereas the rest of AVC interacts with the lipophilic regions of CCR5. *Panel B*, a docked structure of AVC (tube representation) bound to CCR5, illustrating the relative location of AVC within CCR5. Important binding site residues of CCR5 are shown in *wires*. Polar hydrogens are only shown. Note that TM1, 2, and 3 are toward the viewer from the plane and TM6 and 7 are away from the viewer behind the plane.

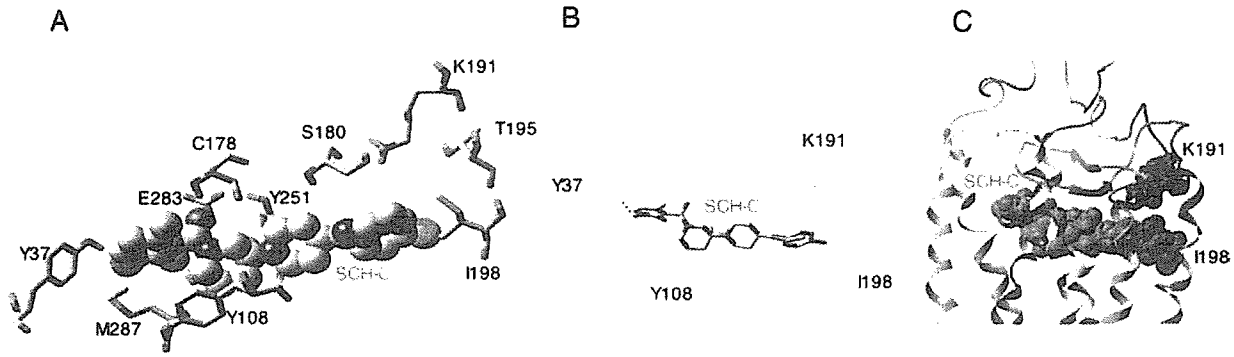

FIGURE 5. **Interactions of SCH-C with CCR5 residues.** *Panel A*, the configuration of SCH-C (shown in CPK) obtained with mutagenesis-based data (Table 1) combined with structural analyses. CCR5 residue orientations (shown in *tubes*) vary from that in Fig. 4 because conformational flexibility of receptors during docking of each inhibitor was taken into account. *Panel B*, Tyr^{37} forms hydrogen bonding interactions with SCH-C, and hence Y37A mutation reduces the binding affinity of SCH-C with CCR5. Note the location of Tyr^{108} and compare its corresponding location for the complex with TAK-779. SCH-C is shown in *tubes* and CCR5 residues in *wires*. Only polar hydrogens are shown in *panels A* and *B*. The molecules are colored by atom types (carbon, *gray*; oxygen, *red*; nitrogen, *blue*; hydrogen, *cyan*; sulfur, *yellow*; and bromine, *green*). *Panel C*, van der Waals interactions of SCH-C (*green*) with Lys^{191} and Ile^{198} (*magenta*). There is tight hydrophobic binding of SCH-C with Ile^{198}. Unlike AVC, Lys^{191} does not form significant interactions with SCH-C.

acts with the lipophilic region of CCR5 (Fig. 4, *A* and *B*). It is of note that AVC has a molecular weight of 614.2, larger than TAK-779 (M_r 531.1) and SCH-C (M_r 557.5), has a substantial hydrophobic contact and fits well inside the large binding cavity within CCR5 as shown in Fig. 4*A*. AVC also forms hydrogen bonds with Cys^{178}, Ser^{180}, Lys^{191}, and Thr^{195} (Fig. 3, *A* and *B*). It is presumed that these interactions with residues in multiple ECLs and the interface of extracellular and transmembrane domains are responsible for the tight binding of AVC to CCR5.

Amino Acid Substitutions Are Likely to Cause Substantial Conformational Changes in ECLs—Substitutions of amino acid residues, which are involved in hydrogen bonding, appear to directly and indirectly disrupt the hydrogen bond networks observed (Fig. 3, *A* and *B*). For example, Gly^{163}, located in TM4, does not interact directly with AVC, but is responsible for maintaining the shape of the binding cavity by its hydrogen bond interactions with Ser^{180} and Lys^{191} (Fig. 3*A*). Thus, the shape of the cavity is most likely altered with G163R substitution, and thereby AVC could lose critical interactions with ECL2 and TM5. In contrast, it was found that G163R exerts minimal effects on the binding of either SCH-C or TAK-779 to CCR5 (Table 1), potentially because these two inhibitors do not have direct hydrogen bond interactions with the ECL or ECL-TM interface.

As mentioned above, the carboxyl of AVC forms hydrogen bonds with Lys^{191} and Ser^{180} (Fig. 3*A*). The loss of binding with K191A substitution (Table 1) is likely because of the loss of the hydrogen bond with AVC as well as the altered shape of the cavity, which was confirmed by structural analysis of the $CCR5_{K191A}$-AVC complex. Neither SCH-C nor TAK-779 forms hydrogen bonds with Lys^{191} (Fig. 5, *A* and *B*, and Fig. 6*A*), hence it is thought that K191A substitution does not significantly affect the binding affinity of SCH-C or TAK-779 (Table 1). Ile^{198} located in TM5 has hydrophobic interactions with AVC (Fig. 3*C*). SCH-C and TAK-779 were predicted to have hydrogen bond interactions with Tyr^{37} located in TM1 (Fig. 5, *A* and *B*, and Fig. 6, *A* and *B*), whereas there appear to be no such interactions with AVC (Fig. 3*B*). This is consistent with the observation that Y37A substitution drastically changed the binding affinity of SCH-C and TAK-779 to CCR5 (Table 1). Ile^{198} forms a hydrophobic contact with SCH-C (Fig. 5*C*), although not much with TAK-779, which well explains the reason I198A reduces the K_D value of SCH-C with CCR5 but not that of TAK-

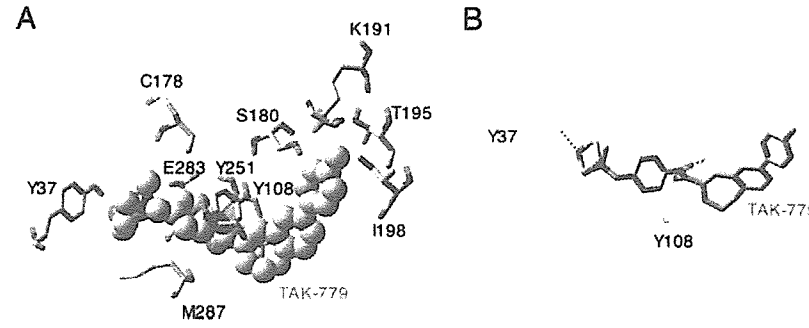

FIGURE 6. **Interactions of TAK-779 with CCR5 residues.** *Panel A*, the configuration of TAK-779 within the CCR5 binding pocket. *Panel B*, Tyr^{37} forms a hydrogen bonding interaction with TAK-779. Note the orientation of Tyr^{108} in comparison to the complex of CCR5 with SCH-C. Tyr^{108} forms π-π and hydrogen bond interactions with TAK-779 and represents a critical residue in agreement with the mutagenesis-based results (Table 1). Only polar hydrogens are shown. The molecules are colored by atom types (carbon, *gray*; oxygen, *red*; nitrogen, *blue*; hydrogen, *cyan*; sulfur, *yellow*).

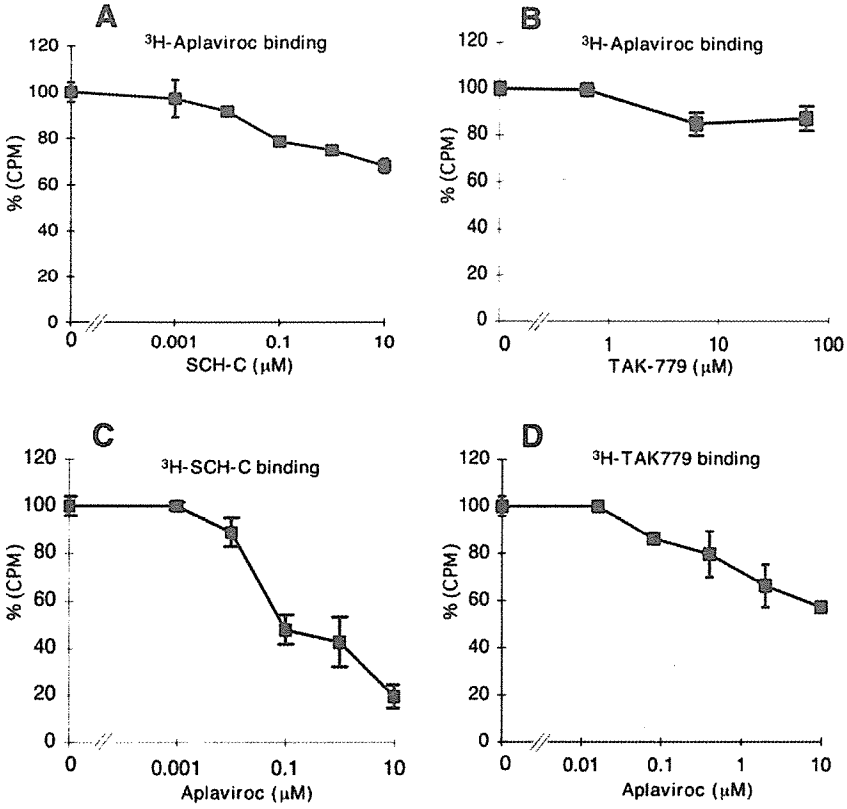

FIGURE 7. **Interactions between CCR5 inhibitors in relation to CCR5.** $CCR5_{WT}$-CHO cells were exposed to [^{3}H]AVC (3 nM; *panels A* and *B*), [^{3}H]SCH-C (3 nM; *panel C*), or [^{3}H]TAK-779 (10 nM; *panel D*), for 15 min, followed by the exposure to various concentrations (from 1 nM to 62.5 μM) of unlabeled SCH-C (*panel A*), TAK-779 (*panel B*), or AVC (*panels C* and *D*) for 30 min. The cells were then thoroughly washed, lysed, and the radioactivity of the lysates counted. All experiments were performed in duplicate and the data shown are mean values ± S.D. The amounts of the [^{3}H]CCR5 inhibitor bound to the cells are shown as mean % control values (each control value was obtained without an indicated unlabeled CCR5 inhibitor).

779 with CCR5 (Table 1). It is also of note that AVC has direct interactions with residues in the extracellular domain and its proximity (Cys^{178}, Ser^{180}, and Lys^{191}) (Fig. 3, *A* and *B*), which should strongly affect the conformation of extracellular loops in comparison to SCH-C and TAK-779, both of which failed to directly interact with the amino acid residues in the extracellular domain. The interaction of HIV-1-gp120 with ECLs is thought to be critical for the establishment of infection, therefore, one can assume that the binding of AVC to CCR5 should result in a significant loss of interactions with gp120, which could explain the significantly greater effect of AVC in blocking viral infectivity, compared with SCH-C and TAK-779. Thus, the data above suggest that the binding pockets are in the same general area within CCR5, however, the binding interactions of the three inhibitors with CCR5 residues substantially differ from each other, in particular between AVC and other two inhibitors.

Interactions between CCR5 Inhibitors in Relation to Their Binding to CCR5—All three CCR5 inhibitors examined in this study possess the properties of allosteric antagonists of CCR5, whereas AVC exerts only partial inhibition of the binding to CCR5 and physiological function of ^{125}I-RANTES in comparison to TAK-779 and SCH-C (11). Moreover, although the binding pocket for these inhibitors are all located in the same hydrophobic cavity within CCR5, their binding profiles substantially differ from each other as discussed above. Therefore, we analyzed the interactions of the three inhibitors in relation to $CCR5_{WT}$. When $CCR5_{WT}$-CHO cells were exposed to [^{3}H]AVC (3 nM) for 15 min, followed by the addition of various concentrations (1 nM to 10 μM) of unlabeled SCH-C, [^{3}H]AVC binding to CCR5 was reduced only moderately, by up to 32% (Fig. 7*A*). When the interaction between [^{3}H]AVC and unlabeled TAK-779 (0.625-62.5 μM) was examined, [^{3}H]AVC binding to CCR5 was not significantly replaced by unlabeled TAK-779 (Fig. 7*B*). On the contrary, when [^{3}H]SCH-C was added first and then unlabeled AVC was added, the binding of [^{3}H]SCH-C to $CCR5_{WT}$-CHO cells was significantly blocked (Fig. 7*C*). These data suggest that AVC effectively replaces [^{3}H]SCH-C and binds to $CCR5_{WT}$. The binding of [^{3}H]TAK-779 was likewise blocked by the addition of unlabeled AVC, although the extent of replacement by AVC was lesser as compared with the case of [^{3}H]SCH-C (Fig. 7*D*).

Role of Amino Acid Residues of CCR5 with Which Aplaviroc Is Associated in HIV-1 Infection and CC-chemokine Binding—In an attempt to define the biological and virological roles of amino acid residues, with which AVC is associated in this binding to CCR5, we selected 15 mutant CCR5-overexpressing CHO cells and examined profiles of sCD4/gp120

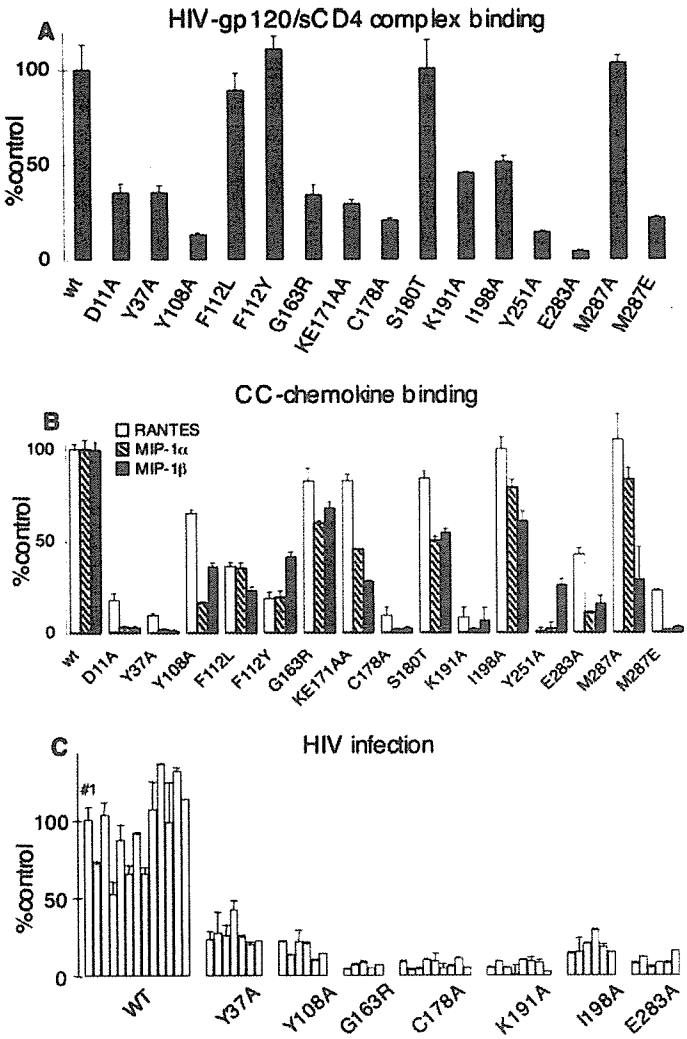

FIGURE 8. **Effects of amino acid substitutions in CCR5 on sCD4/gp120 binding, HIV infection, and CC-chemokine binding.** *Panel A*, profiles of the binding of sCD4/$gp120_{YU2}$ complex to various $CCR5_{MT}$ species overexpressing CHO cells. All values were normalized with the CCR5 expression level of each $CCR5_{MT}$ compared with that of $CCR5_{WT}$ (see "Experimental Procedures"). *Panel B*, profiles of the binding of ^{125}I-RANTES, ^{125}I-MIP-1α, and ^{125}I-MIP-1β to various $CCR5_{MT}$-expressing CHO cell preparations. All values were normalized with the CCR5 expression level of each $CCR5_{MT}$ compared with that of $CCR5_{WT}$. All assays were performed in duplicate or triplicate. *Panel C*, the susceptibility of various $CCR5_{MT}$-overexpressing U373-MAGI cells. For testing each $CCR5_{MT}$-overexpressing cell preparation, multiple clones were examined. In each set of experiments, $CCR5_{WT}$-clone 1 (*solid column*) served as a standard (100%).

binding and CC-chemokine (RANTES, MIP-1α, and MIP-1β) binding profiles. Nine of the 15 mutants were chosen based on the following reasons. Tyr^{108} was chosen because Tyr^{108} is within the aromatic cluster seen in the proximity of TM2 and TM3 and is reported to play a crucial role in the CC-chemokine-elicited activation of CCR5 (35). Y37A and E283A were chosen because Tyr^{37} and Glu^{283} are involved in the binding of the three inhibitors to CCR5 and have been shown to be highly conserved in CC-chemokine receptors including CCR5, CCR2B, CCR3, CCR1, and CCR4 (6). Six more mutants (G163R, C178A, K191A, I198A, Y251A, and M287E) were also chosen, with which the binding affinity of AVC was significantly reduced compared with $CCR5_{WT}$-expressing cells (>5-fold K_D difference) (Table 1). As shown in Fig. 8*A*, all 9 mutations described above decreased the sCD4/gp120 binding to CCR5 compared with that to $CCR5_{WT}$. It was noted that Y108A, Y251A, and E283A substitutions resulted in the greatest reduction of sCD4/gp120 binding.

We further determined the binding profiles of ^{125}I-RANTES, ^{125}I-MIP-1α, and ^{125}I-MIP-1β to the above 9 mutant CCR5-overexpressing CHO cell lines (Fig. 8*B*). In several CHO cell lines, the CC-chemokine binding profile notably differed from the HIV-gp120/sCD4 complex binding profile. Whereas both K191A and I198A substitutions caused moderate reduction in HIV-gp120/sCD4 complex binding (Fig. 8*A*), CC-chemokine binding was fairly preserved in $CCR5_{I198A}$-expressing cells, whereas CC-chemokine binding was almost completely reduced in $CCR5_{K191A}$-expressing cells. The G163R substitution preserved HIV-gp120/sCD4 complex binding by 34%, however, CC-chemokine binding was substantially spared by 68–83%.

We also employed six additional mutant CCR5-overexpressing CHO cells, which showed insignificant to minimal changes (less than 3-fold differences) in their K_D values compared with the K_D value for wild-type CCR5 (Table 1). Two substitutions in the extracellular domain of CCR5, D11A (NH_2 terminus) and KE171AA (ECL2), induced substantial reduction in HIV-gp120/sCD4 complex binding by 65 and 70%, respectively. The F112L, F112Y (both in TM3), S180T (ECL2), and M287A (TM7) substitutions caused no significant changes in K_D values (Table 1) or HIV-gp120/sCD4 complex binding (Fig. 8*A*). These data suggest that amino acid residues in the proximity of the hydrophobic cavity for AVC that do not change K_D values generally do not affect the HIV-gp120/sCD4 complex binding to CCR5. These 6 substitutions, however, caused CC-chemokine binding inhibition at various degrees, suggesting that the profile of the HIV-gp120/sCD4 complex binding to CCR5 differs from that of CC-chemokine binding to CCR5.

We finally generated seven clonal populations of $CD4^+$U373-MAGI cells expressing CCR5 with an amino acid substitution that caused significant reduction in the K_D values of either of the three CCR5 inhibitors and examined their susceptibility to HIV-1_{BaL} infection (Fig. 8*C*). HIV-1_{BaL} effectively infected $CCR5_{WT}$-expressing cells, however, the susceptibility to HIV-1_{BaL} infection was greatly reduced in $CCR5_{Y37A}$-, $CCR5_{Y108A}$-, and $CCR5_{I198A}$-expressing cells and that in $CCR5_{G163R}$-, $CCR5_{C178A}$-, $CCR5_{K191A}$-, and $CCR5_{E283A}$-expressing cells was more greatly limited. These data indicate that the mutations examined in this experiment effectively blocked HIV-1_{BaL} infection, although such mutations, in particular three mutations (G163R, K191A, and I198A), allowed some degree of sCD4/gp120 binding to $CCR5^+$ cells (Fig. 8*A*).

As noted above, the CC-chemokine binding profile notably differed from the profile of HIV-1_{BaL} infection susceptibility in $CCR5_{G163R}$- and $CCR5_{I198A}$-expressing cells. Moreover, moderate levels of chemokine binding were seen in $CCR5_{Y108A}$- and $CCR5_{E283A}$-expressing cells, whereas the least infection occurred in these cells. It should be of note that when we examined what ensued upon the binding of RANTES to $CCR5_{G163R}$-expressing cells, it was found that the level of Ca^{2+} flux that occurred in those cells was comparable with that in $CCR5_{WT}$-expressing cells following stimulation with RANTES.[3]

These data, taken together, suggest that the binding affinity of AVC seen with CCR5 variants generally paralleled the HIV-gp120/sCD4 complex binding affinity to mutant CCR5s, although it is of note that further fine-tuned analysis with greater numbers of CCR5 mutants is required for full understanding of the interactions among the HIV-gp120/sCD4 complex, CC-chemokines, and CCR5 inhibitors. The data also suggest that certain conformational changes caused by amino acid substitutions (*e.g.* at Tyr^{108}, Gly^{163}, or Ile^{198} residues of CCR5) might substantially reduce HIV-1 infection without significantly affecting physiological CC-chemokine-CCR5 interactions.

[3] K. Maeda, H. Nakata, T. Miyakawa, and H. Mitsuuya, unpublished data.

DISCUSSION

In the present study, we examined the structural and molecular interactions between CCR5 and three CCR5 inhibitors, AVC, SCH-C and TAK-779. When we exploited site-directed mutagenesis by generating a panel of mutant CCR5-expressing cells, and determined the K_D values of each CCR5 inhibitor with each mutant CCR5 species, the K_D values compiled corroborated our previous results obtained using the mAb replacement assay (11). We found that the binding affinity of AVC to wild-type CCR5 ($CCR5_{WT}$) was the greatest with a K_D value of 2.9 nM as compared with SCH-C and TAK-779 with K_D values of 16.0 and 30.2 nM, respectively (Table 1). It was also noted that the number of mutations that affected the binding of AVC was greater than in the cases of TAK-779 and SCH-C (Table 1). Moreover, the amino acid substitutions with which AVC turned out to have different K_D values were mostly located in the second extracellular loop (ECL2) and its interface with TM4 (Gly^{163}), or TM5 (Lys^{191}). By contrast, with regard to SCH-C and TAK-779, no substantially different K_D values were obtained with amino acid substitutions in ECL2 (Table 1). The data suggest that not only the binding interactions but also the molecular size and/or bulkiness of AVC are related to the different numbers of K_D-affecting mutations and different profile of K_D values obtained and that AVC forms substantial hydrophobic contacts with and fits well inside the hydrophobic cavity within CCR5 (Fig. 4*A*). It was also thought that such tight interactions of AVC with residues in ECLs and the interface of extracellular and transmembrane domains of CCR5 are responsible for the greater binding affinity of AVC to CCR5 as compared with two other inhibitors.

It was intriguing that certain amino acids such as Gly^{163} and Lys^{191} formed critical hydrogen bond networks in the interaction of AVC and CCR5 (Fig. 3, *A* and *B*). It was thought, therefore, that the amino acid substitutions in such positions dramatically altered the binding affinity of AVC to CCR5. It is also noteworthy that Cys^{178} of ECL2 is presumed to form a putative disulfide bridge with Cys^{101} of ECL1 and to be critical for the conformation of CCR5 (34). In the present study, C178A substitution, which should disrupt the putative disulfide bridge and cause significant conformational changes in both ECL1 and ECL2, nullified the CCR5 binding affinity of AVC, but not of SCH-C or TAK-779 (Table 1). In this respect, the lesser interactions of SCH-C and TAK-779 with extracellular domains (Table 1) are likely responsible for the lack of influence of the C178A substitution on the binding affinity of SCH-C and TAK-779, corroborating the notion that mutations in ECL2 did not alter the binding of SCH-C and TAK-779 to CCR5 (Table 1).

Two events are likely involved in the reduced binding of inhibitors to CCR5 with an amino acid substitution(s): (i) the alteration of direct interaction, if present, between the amino acid residue and the inhibitor and/or (ii) an allosteric effect(s) in which there is a significant conformational change(s) of CCR5 either near or distant from the mutated residue. In this respect, in the present work, we have shown that multiple hydrogen bond networks are important for the binding of AVC to CCR5 (Fig. 3, *A* and *B*). Some residues such as Lys^{191} directly interact with AVC, and hence mutations that lose this direct interaction are very likely responsible for the loss of binding. The lack of drastic changes in the binding of SCH-C and TAK-779, which are not predicted to directly interact with Lys^{191}, also supports this inference. Gly^{163}, however, does not directly bind to AVC but is a critical part of the Gly^{163}-Ser^{180}-Lys^{191}-Thr^{195} hydrogen network (Fig. 3*A*). Our molecular modeling, however, indicates that arginine at position 163 does not form hydrogen bonds with Ser^{180} or Lys^{191}. This alteration in the hydrogen bond network probably changes the shape of the cavity in the ECL2-TM4-TM5 region (an allosteric effect near the mutated residue) and results in reduced binding of AVC to $CCR5_{G163R}$. Mutation at residue 283 might be an example of the one causing an allosteric conformational change(s) distant from the mutated residue. Only AVC is predicted to directly interact with Glu^{283}, but a E283A mutation results in significant loss of binding for all three inhibitors examined. Thus, it is thought that certain amino acid substitutions reduce the binding of an inhibitor even though they are not directly interacting with the inhibitor. It is also of note that mutations at certain residues directly interacting with an inhibitor do not always cause significant loss of binding if CCR5 does not undergo a conformational change(s) or takes an alternate conformation that is not unfavorable for inhibitor binding.

Because a crystal structure of CCR5 is not available, unlike other targets for intervention of HIV infection including HIV reverse transcriptase (36), in the present study, in an attempt to conduct structural analyses of the interactions of CCR5 inhibitors with various mutant CCR5 species, an initial structural model of CCR5 was generated using homology modeling based on the crystal structure of bovine rhodopsin (23). The present approach of combining the site-directed mutagenesis-based data (Table 1) and molecular modeling should be a valuable strategy for gaining structural insights for membrane-bound proteins for which x-ray crystal structures are not as yet available. The CCR5-inhibitor complex structures were defined by iterative optimization of CCR5 and inhibitor structures. Mutated CCR5 structures were also defined and optimized based on the wild-type CCR5 structure, and minimized structures of various CCR5 mutants were used as starting structures for obtaining docked complexes of mutated CCR5 with inhibitors. It is of note that in the present study, our modeling study was combined and fine-tuned with the results of the saturation binding assay using a panel of mutant CCR5-expressing cells and tritiated CCR5 inhibitors and the resultant configuration and orientation of inhibitors docked within the hydrophobic cavity of CCR5 yielded a consistent analysis of the structure-activity data. The conformations of CCR5 without an inhibitor and CCR5 bound to an inhibitor are likely to be substantially different from each other because conformational changes are expected to occur upon inhibitor binding to CCR5. Thus, the conformational flexibility of both inhibitors and CCR species were taken into account in our analysis. In this regard, our ongoing analyses of binding affinity profiles using different ^{3}H-labeled CCR5 inhibitors and an expanded panel of mutant CCR5-expressing cell lines should further illuminate the intramolecular and intermolecular interactions of CCR5 and CCR5 inhibitors.

We also examined the binding profile of CCR5 inhibitors when one inhibitor was added to CCR5-overexpressing cells, followed by the addition of the second inhibitor (Fig. 7). Interestingly, when AVC first bound to CCR5 and SCH-C or TAK-779 was subsequently added, both SCH-C and TAK-779 only partially displaced AVC (Fig. 7, *A* and *B*). However, when SCH-C or TAK-779 first bound to CCR5 and AVC was subsequently added, SCH-C and TAK-779 were substantially displaced by AVC (Fig. 7, *C* and *D*). This ineffective displacement of AVC once bound to $CCR5_{WT}$ by SCH-C and TAK-779 could be explained by the difference of their K_D values (2.9 nM for AVC, 16 nM for SCH-C, and 30.2 nM for TAK-779 as illustrated in Table 1). However, it is of note that both SCH-C and TAK-779 failed to displace AVC even with very high concentrations: 3,333-fold (10 μM; Fig. 7*A*) and 20,833-fold (62.5 μM; Fig. 7*B*), respectively, greater than the [^{3}H]AVC concentration (3 nM). Thus, only the difference in K_D values among the three inhibitors unlikely fully explains the failure of AVC replacement by SCH-C and TAK-779. In this regard, a possible explanation is that AVC induces a series of significant conformational changes in CCR5 and, upon the completion of its stable lodging within the hydrophobic cavity within $CCR5_{WT}$, the binding and/or entry into CCR5 of the second inhibitor is

hindered and the interaction between AVC and the second inhibitor added is no longer merely competitive. Although the data of displacement experiments using two CCR5 inhibitors discussed above may not offer a clear mechanistic explanation at present due to the limitation of the currently available methodologies, the data may have a clinical relevance in the future because more than one CCR5 inhibitor may be simultaneously administered when multiple CCR5 inhibitors are introduced in the therapy of AIDS. It is also noteworthy that the tight CCR5 binding profile of AVC is presumably related to the extensive and prolonged CCR5 occupancy observed in phytohemagglutinin-activated peripheral blood mononuclear cells ($t_{1/2} \sim 9$ h) (12) and in circulating lymphocytes in HIV-1-negative and HIV-1-positive individuals ($t_{1/2}$ of 69–152 h depending on different AVC doses), a potentially favorable feature that could enable once daily (*QD*) or twice daily (*BID*) administration of AVC.

In the present study, we observed that amino acid mutations within the transmembrane domains such as Y108A, G163R, and I198A exerted only minimal or moderate effects on the binding of CC-chemokines to CCR5 (Fig. 8*B*), whereas they caused a substantial reduction in HIV-1-gp120/CD4 complex binding to CCR5 (Fig. 8*A*) and a more drastic reduction in the susceptibility to HIV-1 infection (Fig. 8*C*). It is possible that the molecular size of the gp120/CD4 complex is far greater and its interactions with CCR5 are more extensive compared with the case of CC-chemokines, and therefore, the process for establishing HIV-1 infection is more extensively affected by such amino acid substitutions in comparison to CCR5 binding of CC-chemokines and the ensuing signal transduction. In this regard, a large body of literature has shown that CCR5 regions to which the envelope glycoproteins of HIV-1 bind are functionally and structurally quite different from those to which CC-chemokines bind (19–21, 32, 33). Wu *et al.* (20) and Lee *et al.* (21) demonstrated that a group of NH_2 terminus-specific CCR5 monoclonal antibodies did not block the binding of or Ca^{2+} flux induction by CC-chemokines, although ECL2-specific monoclonal antibodies effectively block the binding of CC-chemokines and their Ca^{2+} flux induction. Navenot *et al.* (33) subsequently confirmed these notions and further demonstrated that a CCR5 chimera with the NH_2 terminus of CXCR2 bound MIP-1α with an affinity similar to that of $CCR5_{WT}$. In contrast, both NH_2 terminus- and ECL2-specific mAbs reportedly blocked efficiently the binding of gp120 to CCR5 although the latter mAbs caused superior inhibition (20, 21). These previously published data strongly suggest that the interactions of CCR5 with HIV-1-glycoproteins involve multiple CCR5 domains and consist of more complex processes, whereas those with CC-chemokines involve fewer CCR5 domains and potentially fewer processes. Thus, this implies that the intervention of HIV-1 infection without interrupting physiological CC-chemokine/CCR5 interactions should be feasible. Indeed, AVC does not potently block the physiologic CC-chemokine/CCR5 interactions, although it highly efficiently suppresses the infection of HIV-1 with IC_{50} values of subnanomolar concentrations (11).

Taken together, mutations associated with AVC binding to CCR5 decreased gp120 binding to CCR5 and the susceptibility to HIV-1 infection, whereas mutations in TM4 and TM5 that also decreased gp120 binding and HIV-1 infectivity had less effects on the binding of CC-chemokines, suggesting that CCR5 inhibition targeting appropriate regions might render the inhibition highly HIV-1-specific, preserving the CC chemokine-CCR5 interactions. The present data should not only help design more potent and HIV-1-specific CCR5 inhibitors, but also should give new insights into the dynamics of CC-chemokine-CCR5 interactions and the mechanisms of CCR5 involvement in the process of cellular entry of HIV-1.

Acknowledgments— We thank Steve LaFon, James Demarest, Alphonso Nillas, Larry Boone, Yashuhiro Koh, Yosuke Maeda, and Philip Yin for helpful discussion and/or critical reading of the manuscript. We also thank the Center for Information Technology, National Institutes of Health, for providing computational resources.

REFERENCES

1. Fauci, A. S. (2003) *Nat. Med.* **9,** 839–843
2. Mitsuya, H., and Erickson, J. (1999) in *Textbook of AIDS Medicine* (Merigan, T. C., Bartlet, J. G., and Bolognesi, D., eds) pp. 751–780, Williams and Wilkins, Baltimore
3. Siliciano, J. D., Kajdas, J., Finzi, D., Quinn, T. C., Chadwick, K., Margolick, J. B., Kovacs, C., Gange, S. J., and Siliciano, R. F. (2003) *Nat. Med.* **9,** 727–728
4. Richman, D. D. (2001) *Nature* **410,** 995–1001
5. Department of Health and Human Services (DHHS) (2005) *Guidelines for the Use of Antiretroviral Agents in HIV-1-infected Adults and Adolescents*
6. Raport, C. J., Gosling, J., Schweickart, V. L., Gray, P. W., and Charo, I. F. (1996) *J. Biol. Chem.* **271,** 17161–17166
7. Alkhatib, G., Combadiere, C., Broder, C. C., Feng, Y., Kennedy, P. E., Murphy, P. M., and Berger, E. A. (1996) *Science* **272,** 1955–1958
8. Deng, H., Liu, R., Ellmeier, W., Choe, S., Unutmaz, D., Burkhart, M., Di Marzio, P., Marmon, S., Sutton, R. E., Hill, C. M., Davis, C. B., Peiper, S. C., Schall, T. J., Littman, D. R., and Landau, N. R. (1996) *Nature* **381,** 661–666
9. Trkola, A., Dragic, T., Arthos, J., Binley, J. M., Olson, W. C., Allaway, G. P., Cheng-Mayer, C., Robinson, J., Maddon, P. J., and Moore, J. P. (1996) *Nature* **384,** 184–187
10. Wu, L., Gerard, N. P., Wyatt, R., Choe, H., Parolin, C., Ruffing, N., Borsetti, A., Cardoso, A. A., Desjardin, E., Newman, W., Gerard, C., and Sodroski, J. (1996) *Nature* **384,** 179–183
11. Maeda, K., Nakata, H., Koh, Y., Miyakawa, T., Ogata, H., Takaoka, Y., Shibayama, S., Sagawa, K., Fukushima, D., Moravek, J., Koyanagi, Y., and Mitsuya, H. (2004) *J. Virol.* **78,** 8654–8662
12. Nakata, H., Maeda, K., Miyakawa, T., Shibayama, S., Matsuo, M., Takaoka, Y., Ito, M., Koyanagi, Y., and Mitsuya, H. (2005) *J. Virol.* **79,** 2087–2096
13. Baba, M., Nishimura, O., Kanzaki, N., Okamoto, M., Sawada, H., Iizawa, Y., Shiraishi, M., Aramaki, Y., Okonogi, K., Ogawa, Y., Meguro, K., and Fujino, M. (1999) *Proc. Natl. Acad. Sci. U. S. A.* **96,** 5698–5703
14. Strizki, J. M., Xu, S., Wagner, N. E., Wojcik, L., Liu, J., Hou, Y., Endres, M., Palani, A., Shapiro, S., Clader, J. W., Greenlee, W. J., Tagat, J. R., McCombie, S., Cox, K., Fawzi, A. B., Chou, C. C., Pugliese-Sivo, C., Davies, L., Moreno, M. E., Ho, D. D., Trkola, A., Stoddart, C. A., Moore, J. P., Reyes, G. R., and Baroudy, B. M. (2001) *Proc. Natl. Acad. Sci. U. S. A.* **98,** 12718–12723
15. Gribble, G. W. (1975) *J. Chem. Soc. Chem. Commun.* 535–541
16. Evans, E. A. (1974) in *Tritium and Its Compounds* (Evans, E. A., ed) pp. 271–317, J. Wiley and Sons, New York
17. Maeda, K., Yoshimura, K., Shibayama, S., Habashita, H., Tada, H., Sagawa, K., Miyakawa, T., Aoki, M., Fukushima, D., and Mitsuya, H. (2001) *J. Biol. Chem.* **276,** 35194–35200
18. Maeda, Y., Foda, M., Matsushita, S., and Harada, S. (2000) *J. Virol.* **74,** 1787–1793
19. Siciliano, S. J., Kuhmann, S. E., Weng, Y., Madani, N., Springer, M. S., Lineberger, J. E., Danzeisen, R., Miller, M. D., Kavanaugh, M. P., DeMartino, J. A., and Kabat, D. (1999) *J. Biol. Chem.* **274,** 1905–1913
20. Wu, L., LaRosa, G., Kassam, N., Gordon, C. J., Heath, H., Ruffing, N., Chen, H., Humblias, J., Samson, M., Parmentier, M., Moore, J. P., and Mackay, C. R. (1997) *J. Exp. Med.* **186,** 1373–1381
21. Lee, B., Sharron, M., Blanpain, C., Doranz, B. J., Vakili, J., Setoh, P., Berg, E., Liu, G., Guy, H. R., Durell, S. R., Parmentier, M., Chang, C. N., Price, K., Tsang, M., and Doms, R. W. (1999) *J. Biol. Chem.* **274,** 9617–9626
22. Maeda, Y., Venzon, D. J., and Mitsuya, H. (1998) *J. Infect. Dis.* **177,** 1207–1213
23. Palczewski, K., Kumasaka, T., Hori, T., Behnke, C. A., Motoshima, H., Fox, B. A., Le Trong, I., Teller, D. C., Okada, T., Stenkamp, R. E., Yamamoto, M., and Miyano, M. (2000) *Science* **289,** 739–745
24. Halgren, T. A., Murphy, R. B., Friesner, R. A., Beard, H. S., Frye, L. L., Pollard, W. T., and Banks, J. L. (2004) *J. Med. Chem.* **47,** 1750–1759
25. Xiang, Z., and Honig, B. (2001) *J. Mol. Biol.* **311,** 421–430
26. Kaminski, G. A., Friesner, R. A., Tirado-Rives, J., and Jorgensen, W. J. (2001) *J. Phys. Chem. B* **105,** 6474–6487
27. Friesner, R. A., Banks, J. L., Murphy, R. B., Halgren, T. A., Klicic, J. J., Mainz, D. T., Repasky, M. P., Knoll, E. H., Shelley, M., Perry, J. K., Shaw, D. E., Francis, P., and Shenkin, P. S. (2004) *J. Med. Chem.* **47,** 1739–1749
28. Exner, T. E., Keil, M., Moeckel, G., and Brickmann, J. (1998) *J. Mol. Model* **4,** 340–343
29. Viswanadhan, V. N., Ghose, A. K., Revankar, G. R., and Robins, R. K. (1989) *J. Chem. Inf. Comput. Sci.* **29,** 163–172

30. Dragic, T., Trkola, A., Thompson, D. A., Cormier, E. G., Kajumo, F. A., Maxwell, E., Lin, S. W., Ying, W., Smith, S. O., Sakmar, T. P., and Moore, J. P. (2000) *Proc. Natl. Acad. Sci. U. S. A.* **97,** 5639–5644
31. Tsamis, F., Gavrilov, S., Kajumo, F., Seibert, C., Kuhmann, S., Ketas, T., Trkola, A., Palani, A., Clader, J. W., Tagat, J. R., McCombie, S., Baroudy, B., Moore, J. P., Sakmar, T. P., and Dragic, T. (2003) *J. Virol.* **77,** 5201–5208
32. Dragic, T., Trkola, A., Lin, S. W., Nagashima, K. A., Kajumo, F., Zhao, L., Olson, W. C., Wu, L., Mackay, C. R., Allaway, G. P., Sakmar, T. P., Moore, J. P., and Maddon, P. J. (1998) *J. Virol.* **72,** 279–285
33. Navenot, J. M., Wang, Z. X., Trent, J. O., Murray, J. L., Hu, Q. X., DeLeeuw, L., Moore, P. S., Chang, Y., and Peiper, S. C. (2001) *J. Mol. Biol.* **313,** 1181–1193
34. Blanpain, C., Lee, B., Vakili, J., Doranz, B. J., Govaerts, C., Migeotte, I., Sharron, M., Dupriez, V., Vassart, G., Doms, R. W., and Parmentier, M. (1999) *J. Biol. Chem.* **274,** 18902–18908
35. Govaerts, C., Bondue, A., Springael, J. Y., Olivella, M., Deupi, X., Le Poul, E., Wodak, S. J., Parmentier, M., Pardo, L., and Blanpain, C. (2003) *J. Biol. Chem.* **278,** 1892–1903
36. Sarafianos, S. G., Das, K., Hughes, S. H., and Arnold, E. (2004) *Curr. Opin. Struct. Biol.* **14,** 716–730
37. Sparks, S., Adkison, K., Shachoy-Clark, A., Piscitelli, S., and Demarest, J. (2005) *12th Conference on Retroviruses and Opportunistic Infections, Boston, February 22–25, 2005*, Abstr. 77, Foundation for Retrovirology and Human Health, Alexandria, VA
38. Lalezari, J., Thompson, M., Kumar, P., Piliero, P., Davey, R., Murtaugh, T., Patterson, K., Shachoy-Clark, A., Adkinson, A., Demarest, J., Sparks, S., Fang, L., Lou, Y., Berrey, M., and Piscitelli, S. (2004) *44th Interscience Conference on Antimicrobial Agents and Chemotherapy, Boston, February 22–25, 2005*, Abstr. H-1137b, Foundation for Retrovirology and Human Health, Alexandria, VA

Journal of Infection (2006) 53, e167–e170

ELSEVIER

BRITISH INFECTION SOCIETY

www.elsevierhealth.com/journals/jinf

CASE REPORT

AIDS-related cerebral toxoplasmosis with hyperintense foci on T1-weighted MR images: A case report

T. Maeda [a,c,*], T. Fujii [b,c], T. Matsumura [b,c], T. Endo [c], T. Odawara [c], D. Itoh [d], Y. Inoue [d], T. Okubo [d], A. Iwamoto [a,b,c], T. Nakamura [c]

[a] *International Research Center for Infectious Diseases, The Institute of Medical Science, The University of Tokyo, 4-6-1 Shirokanedai, Minato-ku, Tokyo 108-8639, Japan*
[b] *Division of Infectious Diseases, Advanced Clinical Research Center, The Institute of Medical Science, The University of Tokyo, 4-6-1 Shirokanedai, Minato-ku, Tokyo 108-8639, Japan*
[c] *Department of Infectious Diseases and Applied Immunology, Research Hospital, The Institute of Medical Science, The University of Tokyo, 4-6-1 Shirokanedai, Minato-ku, Tokyo 108-8639, Japan*
[d] *Department of Radiology, Research Hospital, The Institute of Medical Science, The University of Tokyo, 4-6-1 Shirokanedai, Minato-ku, Tokyo 108-8639, Japan*

Accepted 8 December 2005
Available online 26 January 2006

KEYWORDS
Toxoplasmosis;
MRI;
AIDS

Summary The neuroradiological findings are helpful for the diagnosis of toxoplasmic encephalitis. The T1 hypersignal intensity foci on brain magnetic resonance (MR) images without contrast enhancement are presented and can be a pathognomonic sign of this disease.

Introduction

Most toxoplasmic encephalitis is opportunistic infection complicated with the acquired immunodeficiency syndrome (AIDS) and immunosuppressive conditions. The diagnosis of this disease is difficult because of the incompetence of the serological examination for the immunocompromised patients.[1] Although the direct detection method for the pathogen by polymerase chain reaction (PCR) using the cerebrospinal fluid (CSF) has high specificity, the sensitivity of this method is insufficient for definitive diagnosis.[2] We, therefore, have to synthetically diagnose with clinical symptoms, signs, laboratory data, neuroradiological images and the response to anti-toxoplasmosis therapy.

We report here our experience of a unique MR imaging finding of toxoplasmic encephalitis in an

* Corresponding author. International Research Center for Infectious Diseases, The Institute of Medical Science, The University of Tokyo, 4-6-1 Shirokanedai, Minato-ku, Tokyo 108-8639, Japan. Tel.: +81 3 5449 5338; fax: +81 3 5449 5427.
E-mail address: tmaeda@ims.u-tokyo.ac.jp (T. Maeda).

0163-4453/$30
doi:10.1016/j.jinf.2005.12.006

AIDS patient and emphasize the hyperintense foci on T1-weighted MR images that can be one of the pathognomonic MR images of this disease.

Case report

A 44-year-old man with disturbance of consciousness and respiratory insufficiency was admitted to our hospital in April 2005. His consciousness had been rapidly deteriorated and he developed coma 2–3 days before hospitalization. Serological tests of HIV antibodies and *Toxoplasma gondii* IgG antibody were positive, but the *T. gondii* IgM antibody was not detected. The concentration of HIV RNA in plasma was 120,000 copies/ml and the CD 4 cell count was 8 μl. The chest X-ray showed bilateral ground glass shadow and *Pneumocystis jiroveci* (carinii) was detected from bronchoalveolar lavage (BAL) fluid. CSF showed mild elevated protein level of 65 mg/dl and pleocytosis, and the opening pressure was over 300 mmH_2O. No malignant cells or microorganisms were detected. *T. gondii* B1-gene fragment was detected by PCR using CSF, therefore, the diagnosis of an AIDS case with toxoplasmic encephalitis was made.[3]

MRI of the brain showed multiple high intensity lesions on T2-weighted image (Fig. 1a) and the corresponding T1-wighted image showed low intensity lesions. Contrast enhanced T1-weighted images showed multiple nodular and ring enhancement lesions.

The chemotherapy with trimethoprim/sulfamethoxazole (TMP/SMX) was very effective and the patient's consciousness level was improved gradually. *P. jiroveci* pneumonia was also cured. MR imaging after 4 weeks of treatment demonstrated that the multiple nodular lesions on T1 and T2-weighted images had significantly been reduced. After 8 weeks of treatment, the contrast enhanced T1-weighted images showed only residual small lesions without contrast enhancement. Interestingly, the hypersignal intensity foci appeared at bilateral basal ganglia obviously after 2 weeks of treatment on the non-enhanced T1-weighted images (Fig. 1b). Corresponding computed tomography (CT) image did not show hemorrhagic or calcified densities (Fig. 1c). These T1 hypersignal intensity foci regressed gradually along with anti-toxoplasmic chemotherapy in proportion to other mass lesions. The T2* (star)-weighted image, which can detect the hemosiderin deposition as hypointensity lesion, operated after 12 weeks of treatment showed no hypointensity at corresponding T1 hypersignal intensity foci on basal ganglia (Fig. 1d).[4] We concluded that the toxoplasmic encephalitis showed the hypersignal intensity foci on T1-weighted MR imaging without hemorrhage or calcification.

Discussion

Toxoplasmic encephalitis progresses rapidly and is life threatening to immunocompromised patients. Therefore, we often have to start the anti-toxoplasmosis therapy when this encephalitis is suspected on the neuroradiologic images and laboratory data. Typically, the toxoplasmic encephalitis lesions on MRI studies appear as T2 hypersignal intensity foci and T1 hypo-isosignal intensity foci, and reveal a rim of enhancement surrounding the edema on contrast enhanced T1-weighted images. Nevertheless, even characteristic foci on these MR images are not pathognomonic. Since the differential diagnosis of toxoplasmic encephalitis from other infections or CNS lymphoma is difficult, improvement in the diagnostic methods is an urgent necessity.

In our case, the toxoplasmic encephalitis was diagnosed with the highly specific PCR and confirmed by the response to anti-toxoplasmosis therapy. Brain MRI revealed unusual findings, T1 hypersignal intensity foci, accompanied by typical multiple high intense lesions on T2-weighted image during the treatment. These unique MR findings have been reported on only a few cases of non-HIV/AIDS-related toxoplasmic encephalitis. Terada et al.[5] reported a case of toxoplasmic encephalitis after stem cell transplantation with T1 hypersignal intensity foci. Autopsy revealed the disseminated toxoplasmosis, and coagulative necrosis without hemorrhage or calcification was revealed at corresponding T1 hypersignal intensity foci by neuropathological study. In another post-bone marrow transplantation case, inflammatory and vascular changes without hemorrhage appeared to be the cause of iso or hypersignal intensity rings by the stereotactic biopsy of T1 hypersignal intensity foci.[6] On the other hand, Navia et al.[7] demonstrated that the T1 hypersignal intensity foci were caused by coagulative necrosis with lipid-laden macrophages. The pathophysiological and neuroradiological mechanisms to create these MRI findings are far from clear yet. The reason why the T1 hypersignal intensity foci tend to localize in the basal ganglia is not clear either.[5,6]

CNS lymphoma, which is important for the distinction from toxoplasmic encephalitis, shows T1 hypo-isosignal intensity foci and never shows T1 hypersignal intensity foci except subacute

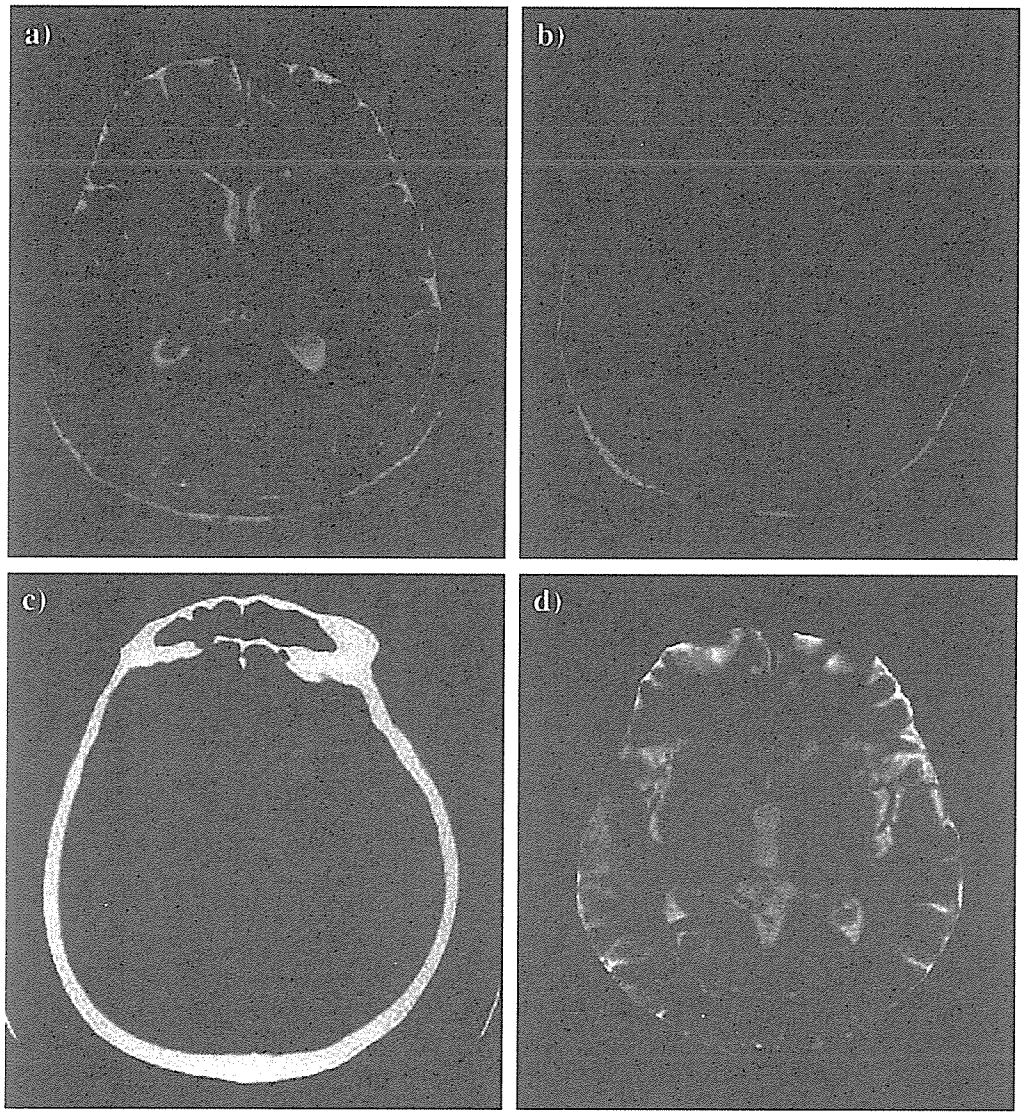

Figure 1 (a) The T2-weighted magnetic resonance image presented multiple high intense lesions. (b) Non-enhanced T1-weighted image showed hypersignal intensity foci at bilateral basal ganglia. (c) The corresponding CT image showed non-hemorrhagic or non-calcified density. (d) The T2* (star)-weighted image showed non-hemorrhagic observations at basal ganglia.

hemorrhage with hypervascular CNS lymphoma.[8,9] However, the CT imaging and T2* (star)-weighted MR imaging can simply distinguish it from the toxoplasmic T1 hypersignal intensity foci without hemorrhage or calcification.

We reported here the unique MRI findings, T1 hypersignal intensity foci, without hemorrhage or calcification on HIV/AIDS-related toxoplasmic encephalitis. It will be helpful for the diagnosis of toxoplasmic encephalitis and may be a pathognomonic finding. Unfortunately, since this report we are yet to experience another case of toxoplasmic encephalitis, but we would like to continue to explore this unique MRI findings of this disease.

Acknowledgement

This work was partly supported by the Special Coordination Funds for Promoting Science and Technology of MEXT: strategic cooperation to control emerging and reemerging infections and grants for AIDS research from the Ministry of Health, Labor and Welfare of Japan.

References

1. Luft BJ, Brooks RG, Conley FK, McCabe RE, Remington JS. Toxoplasmic encephalitis in patients with acquired immune deficiency syndrome. *JAMA* 1984;**252**:913–7.

2. Cingolani A, De Luca A, Ammassari A, Murri R, Linzalone A, Grillo R, et al. PCR detection of *Toxoplasma gondii* DNA in CSF for the differential diagnosis of AIDS-related focal brain lesions. *J Med Microbiol* 1996;**45**:472–6.
3. Castro KG, Ward JW, Slutsker L, Buehler JW, Jaffe HW, Ruth L, et al. 1993 revised classification system for HIV infection and expanded surveillance case definition for aids among adolescents and adults. *Morb Mortal Wkly Rep* 1992; **41**:1–19.
4. Bulte JW, Kraitchman DL. Iron oxide MR contrast agents for molecular and cellular imaging. *NMR Biomed* 2004;**17**: 484–99.
5. Terada H, Kamata N, Yokoyama Y, Ohashi K, Akiyama H, Sakamaki H. T1-hypersignal foci in cerebral toxoplasmosis. *Riv Neuroradiol* 2001;**14**:665–7 [Case report].
6. Dietrich U, Maschke M, Dorfler A, Prumbaum M, Forsting M. MRI of intracranial toxoplasmosis after bone marrow transplantation. *Neuroradiology* 2000;**42**:14–8.
7. Navia BA, Petito CK, Gold JW, Cho ES, Jordan BD, Price RW. Cerebral toxoplasmosis complicating the acquired immune deficiency syndrome: clinical and neuropathological findings in 27 patients. *Ann Neurol* 1986;**19**:224–38.
8. Jenkins CN, Colquhoun IR. Characterization of primary intracranial lymphoma by computed tomography: an analysis of 36 cases and a review of the literature with particular reference to calcification haemorrhage and cyst formation. *Clin Radiol* 1998;**53**:428–34 [Review].
9. Rubenstein J, Fischbein N, Aldape K, Burton E, Shuman M. Hemorrhage and VEGF expression in a case of primary CNS lymphoma. *J Neurooncol* 2002;**58**:53–6.